Mon. Not. R. Astron. Soc. **340,** 115–138 (2003)

Observational implications of a plerionic environment for gamma-ray bursts

Dafne Guetta[1]★ and Jonathan Granot[2]★

[1]*Osservatorio astrofisico di Arcetri, L. E. Fermi 5, Firenze, Italy*
[2]*Institute for Advanced Study, Olden Lane, Princeton, NJ 08540, USA*

Accepted 2002 November 12. Received 2002 November 6; in original form 2002 August 7

ABSTRACT

We consider the possibility that at least some gamma-ray burst (GRB) explosions take place inside pulsar wind bubbles (PWBs), in the context of the supranova model, where initially a supernova explosion takes place, leaving behind a supra-massive neutron star (SMNS), which loses its rotational energy on a time-scale of months to tens of years and collapses to a black hole, triggering a GRB explosion. The most natural mechanism by which the SMNS can lose its rotational energy is through a strong pulsar-type wind, between the supernova and the GRB events, which is expected to create a PWB. We analyse in some detail the observational implications of such a plerionic environment on the afterglow and prompt GRB emissions and the prospect for direct detection of the plerion emission. We find that for a simple spherical model, GRBs with iron lines detected in their X-ray afterglow should not have a detectable radio afterglow and should have small jet break times and non-relativistic transition times, in disagreement with observations for some of the GRBs with X-ray lines. These discrepancies with the observations may be reconciled by resorting to a non-spherical geometry, where the PWB is elongated along the polar axis. We find that the emission from the PWB should persist well into the afterglow, and the lack of detection of such a component provides interesting constraints on the model parameters. Finally, we predict that the inverse Compton upscattering of the PWB photons by the relativistic electrons of the afterglow (external Compton, EC) should lead to high-energy emission during the early afterglow that might explain the GeV photons detected by EGRET for a few GRBs, and should be detectable by future missions such as GLAST.

Key words: radiation mechanisms: non-thermal – shock waves – pulsars: general – stars: winds, outflows – supernova remnants – gamma-rays: bursts.

1 INTRODUCTION

The leading models for gamma-ray bursts (GRBs) involve a relativistic wind emanating from a compact central source. The prompt gamma-ray emission is usually attributed to energy dissipation within the outflow itself, arising from internal shocks within the flow that arise from variability in its Lorentz factor, while the afterglow (AG) emission arises from an external shock that is driven into the ambient medium, as it decelerates the ejected matter (Rees & Mészáros 1994; Sari & Piran 1997). In this so-called 'internal–external' shock model, the duration of the prompt GRB is directly related to the time during which the central source is active. The most popular emission mechanism is synchrotron radiation from relativistic electrons accelerated in the shocks, which radiate in the strong magnetic fields (close to equipartition values) within the shocked plasma. An additional radiation mechanism that may also play some role is synchrotron self-Compton (SSC) scattering, which is the upscattering of the synchrotron photons by the relativistic electrons, to much higher energies.

Progenitor models of GRBs are divided into two main categories. The first category involves the merger of a binary system of compact objects, such as a double neutron star (NS–NS, Eichler et al. 1989), a neutron star and a black hole (NS–BH, Narayan, Paczński & Piran 1992) or a black hole and a helium star or a white dwarf (BH–He, BH–WD, Fryer & Woosley 1998; Fryer, Woosley & Hartmann 1999). The second category involves the death of a massive star. It includes the failed supernova (SN) (Woosley 1993) or hypernova (Paczński 1998) models, where a black hole is created promptly, and a large accretion rate from a surrounding accretion disc (or torus) feeds a strong relativistic jet

★E-mail: dafne@arcetri.astro.it (DG); granot@ias.edu (JG)

in the polar regions. This type of model is known as the collapsar model. An alternative model within this second category is the supranova model (Vietri & Stella 1998), where a massive star explodes in a supernova and leaves behind a supra-massive neutron star (SMNS), which on a time-scale of a few years loses its rotational energy and collapses to a black hole, triggering the GRB event. Long GRBs (with a duration $\gtrsim$2 s) are usually attributed to the second category of progenitors, while short GRBs are attributed to the first category. In all the different scenarios mentioned above, the final stage of the process consists of a newly formed black hole with a large accretion rate from a surrounding torus, and involve a similar energy budget ($\lesssim 10^{54}$ erg).

In this work we perform a detailed analysis of the supranova model, focusing on its possible observational signatures. This aims towards establishing tools that would enable us to distinguish between the supranova model and other progenitor models through observations, and to constrain the model parameter using current observations. The original motivation for the supranova model was to provide a relatively baryon-clean environment for the GRB jet. As it turned out, it also seemed to naturally accommodate the later detection of iron lines in several X-ray afterglows (Lazzati, Campana & Ghisellini 1999; Piro et al. 2000; Vietri et al. 2001).

It was later suggested that the most natural mechanism by which the SMNS can lose its rotational energy is through a strong pulsar-type wind, between the supernova and the GRB events, which typically creates a pulsar wind bubble (PWB), also referred to as a plerion (Königl & Granot 2002, KG hereafter; Inoue, Guetta & Pacini 2003, IGP hereafter). KG suggested that the shocked pulsar wind into which the afterglow shock propagates in this picture may naturally account for the large inferred values of $\epsilon_e \sim 0.1$ and $\epsilon_B \sim 10^{-3}$–0.1 (the fractions of the internal energy in the electrons and in the magnetic field, respectively) that are inferred from fits to afterglow observations (Granot, Piran & Sari 1999; Wijers & Galama 1999; Chevalier & Li 2000; Panaitescu & Kumar 2002). This is attributed to the fact that pulsar winds are believed to largely consist of electron–positron pairs, and have magnetization parameters in the right range. This relaxes the need to generate strong magnetic fields in the shock itself, as is required in other models, where the magnetic field in the external medium (assumed to be either the interstellar medium (ISM) or a stellar wind of a massive star progenitor) is typically too small to account for the values of ϵ_B that are inferred from observations. Another attractive feature of this model, pointed out by IGP is the possible high-energy emission, in the GeV–TeV range, that may result from the upscattering of photons from the plerion by the relativistic electrons in the afterglow shock (external Compton, EC hereafter), and may be detected by GLAST. They have shown that the EC emission can provide a viable explanation for the extended GeV emission seen by EGRET in GRB 940217 (Hurley et al. 1994).

We use a simple spherical model for the PWB. We find that a spherical model cannot accommodate the typical afterglow emission together with the iron line features observed in the X-ray afterglow of some GRBs. However, it was mentioned early on that in order to have a long-lived afterglow emission together with the iron line features, a deviation from spherical symmetry is needed, where the line of sight is relatively devoid of the material producing the iron lines (Lazzati et al. 1999; Vietri et al. 2001). This is required in order to avoid a direct collision of the afterglow shock with the line producing material on an observed time of the order of a day or so. It was later pointed out that a PWB is expected to exist inside the supernova remnant (SNR) shell, which decelerates the afterglow shock at a smaller radius, so that in order for the afterglow to remain relativistic up to a month or more, and produce the iron lines, we need the PWB to be elongated along its rotational axis (KG). In this paper we strengthen this conclusion, and show that in order to produce iron lines with a spherical PWB, its radius must be sufficiently small, resulting in a large density inside the PWB and a high self-absorption frequency implying no radio afterglow, in contrast with observations. We leave the detailed treatment of an elongated PWB to a future work, while in the present work we briefly comment concerning the expected effects of an elongated geometry compared with a spherical one.

In this work we extend the analysis of KG and IGP, and perform detailed calculations of the radiation from the PWB, the prompt GRB and from the afterglow that occurs inside the PWB. We now give a short overview of the structure of the paper, where in each section we stress the original features, new results and the observational constraints on the model. In Section 2 we present our 'PWB' model, introduce the relevant parametrization and model the acceleration of the supernova remnant shell by the shocked pulsar wind. We use a simple spherical geometry and the pulsar wind is assumed to consist of proton and $e^{\pm}$ components with roughly equal energies and a magnetic field. The conditions under which the iron line features that were observed in several X-ray afterglows may be reproduced within the PWB model, are investigated in Section 3. We find that this requires a time delay of $\lesssim$1 yr between the supernova and the GRB events. In Section 4 we perform a detailed study of the plerion emission, including the synchrotron and SSC components, and provide an elaborate description of the relevant Klein–Nishina effect. We also discuss the upper cut-off that is imposed on high-energy photons as a result of pair production with the radiation field of the PWB, go over the prospect for direct detection of the plerion emission and derive observational constraints on the parameters of our model. The effects of the PWB environment on the prompt GRB emission are analysed in Section 5, and we find that the EC from the prompt GRB should typically be very small, but might be detectable for extreme parameters. In Section 6 we discuss the implications of a plerionic environment on the afterglow emission, and introduce the appropriate parametrization. The radial density profile of the PWB is approximated as a power law in radius (KG), $\propto r^{-k}$, where k typically ranges between 0 (similar to an ISM) and 1 (intermediate between an ISM and a stellar wind). The synchrotron, SSC and EC components are calculated and we provide detailed expressions for the break frequencies and flux normalization, for $k = 0, 1$. We also calculate the high-energy emission that is predicted in this model. The results are discussed in Section 7 and in Section 8 we give our conclusions.

2 THE PULSAR WIND BUBBLE

Within the framework of the supranova model, an SMNS (also simply referred to as a pulsar) is formed in a supernova explosion, and then loses a large part of its rotational energy before collapsing to a black hole and triggering the GRB. The most plausible mechanism for this

energy loss is through a pulsar-type wind (KG; IGP). A pulsar wind bubble is formed when the relativistic wind (consisting of relativistic particles and magnetic fields) that emanates from a pulsar is abruptly decelerated (typically, to a Newtonian velocity) in a strong relativistic shock, as a result of interaction with the ambient medium. When a bubble of this type expands inside an SNR, it gives rise to a plerionic SNR, of which the Crab and Vela remnants are prime examples. Motivated by previous works (Rees & Gunn 1974; Kennel & Coroniti 1984; Emmering & Chevalier 1987; KG) we consider in detail a spherical model where the shocked pulsar wind remains largely confined within the SNR. In Section 7 we briefly discuss the possible consequences of some more complicated geometries.

The wind luminosity may be estimated by the magnetic dipole formula (Pacini 1967),

$$L_{\rm w} = \frac{B_*^2 R_*^6 \Omega_*^4}{6c^3} = 7.0\times 10^{44}\left(\frac{B_*}{10^{12}\ {\rm G}}\right)^2\left(\frac{R_*}{15\ {\rm km}}\right)^6\left(\frac{\Omega_*}{10^4\ {\rm s}^{-1}}\right)^4\ {\rm erg\ s}^{-1}, \tag{1}$$

where B_* is the polar surface magnetic field, R_* is the circumferential radius (neglecting the distinction between its equatorial and polar values in this approximation) and Ω_* is the (uniform) angular velocity (the maximum value of which is $\sim 2\times 10^4\ {\rm s}^{-1}$; e.g. Haensel, Lasota & Zdunik 1999). The spin-down time of a rapidly rotating SMNS can be estimated as

$$t_{\rm sd} = \frac{E_{\rm rot}}{L_{\rm w}} \approx 6\left(\frac{\alpha}{0.5}\right)\left(\frac{M_*}{2.5\ {\rm M}_\odot}\right)^2\left(\frac{R_*}{15\ {\rm km}}\right)^{-6}\left(\frac{\Omega_*}{10^4\ {\rm s}^{-1}}\right)^{-3}\left(\frac{B_*}{10^{12}\ {\rm G}}\right)^{-2}\ {\rm yr} \tag{2}$$

(see Vietri & Stella 1998), where $E_{\rm rot} = \alpha\, GM_*^2\Omega_*/2c$ is the portion of the rotational energy of an SMNS of mass M_* and angular velocity Ω_* that needs to be lost before it becomes unstable to collapse.[1] The spin-down time-scale, which sets the time delay between the supernova and GRB events, depends on the physical parameters of the SMNS. Of these parameters, the least constrained is the magnetic field, which is typically expected to be in the range of $\sim 10^{12}$–10^{13} G, and may cause a variation of $\gtrsim 2$ orders of magnitude in $t_{\rm sd}$. There is also a strong dependence on the radius R_*, which depends on its mass M_* and the (uncertain) equation of state, which may account for a change of up to ~ 1 order of magnitude in the scaling of $t_{\rm sd}$. For example, for $R_* = 10$ km, with the values of the other parameters as given in equation (2), we have $t_{\rm sd} \approx 60$ yr. We conclude that the expected range of $t_{\rm sd}$ is from a few weeks to several years.

During $t_{\rm sd}$ the luminosity of the wind is roughly constant and the wind should energize the PWB, depositing an energy of the order of $E_{\rm rot}$. The luminosity of the pulsar wind is divided between its different components: fractions $\xi_{\rm e}$, $\xi_{\rm p}$ and $\sigma_{\rm w}$ in $e^\pm$ pairs, protons and Poynting flux (magnetic field), respectively. The inferred values of $\xi_B = \sigma_{\rm w}/(1+\sigma_{\rm w})$ for PWBs, such as Vela or the Crab, are typically $\sim 10^{-3}$ (Arons 2002), though there are also estimates as high as ~ 1 (Helfand, Gotthelf & Halpern 2001). We shall adopt a fiducial value of $\sigma_{\rm w} = 10^{-3}$, which implies $\xi_{\rm e} + \xi_{\rm p} = 1 - \xi_B \cong 1$. Gallant & Arons (1994) inferred $\xi_{\rm p}/\xi_{\rm e} \sim 2$ for the Crab, and we adopt this estimate for our fiducial values, and use $\xi_{\rm e} = 1/3$ and $\xi_{\rm p} = 2/3$. The inferred values of the Lorentz factor of the pulsar wind are $\gamma_{\rm w} \sim 10^4$–10^7.

The SN ejecta is accelerated by the force exerted owing to the pressure of the expanding PWB, $p_{\rm out}$, at its outer boundary, i.e. at the radius of the SNR, $R_{\rm SNR}$. The pressure is expected to drop by a factor of the order of unity between the radius of the wind termination shock, $R_{\rm s}$, and $R_{\rm SNR}$ (KG), so that $p_{\rm out} \equiv \eta_{\rm p} p_{\rm av}$, where $p_{\rm av} = \eta E_{\rm w}/3V = \eta E_{\rm w}/4\pi R^3$ is the average pressure inside the PWB, η is the fraction of the energy $E_{\rm rot}$ that remains in the PWB, $V = (4\pi/3)R^3$ is the volume of the PWB (which can be different for an elongated PWB) and $E_{\rm w} \approx E_{\rm rot}(t/t_{\rm sd})$ is the energy emitted in the wind up to the time t. As we show below, the PWB is typically fast cooling and the electrons lose all of their internal energy to radiation, implying $\eta \approx \xi_{\rm p} + \xi_B \approx \xi_{\rm p}$. The equation of motion, $M_{\rm SNR}\ddot{R} = 4\pi R^2 p_{\rm out}$, may be written as

$$R\ddot{R} = \frac{\eta_{\rm p}\eta E_{\rm rot}}{M_{\rm SNR} t_{\rm sd}} t. \tag{3}$$

In the case of a non-spherical PWB, $M_{\rm SNR}$ should be replaced by the isotropic equivalent mass, $M_{\rm iso}(\theta) = 4\pi {\rm d}M_{\rm SNR}/{\rm d}\Omega$, and R becomes $R(\theta)$, where θ is the angle from the polar axis. However, the pressure can be taken as being independent of the angle θ, since the shocked pulsar wind is highly subsonic. If $M_{\rm iso}(\theta)$ is smaller near the poles ($\theta \approx 0$) and larger near the equator ($\theta \approx \pi/2$), then even if the SNR shell is initially spherical, the acceleration would be larger near the poles, resulting in a much larger polar radius, $R_{\rm p}$, compared with the equatorial radius, $R_{\rm eq}$: $R_{\rm p} \gg R_{\rm eq}$. This is a natural mechanism that can lead to an elongated geometry for the PWB.

Returning to the spherical case, the acceleration becomes significant at the time $t_{\rm acc}$ (and radius $R_{\rm acc} \approx v_0 t_{\rm acc}$) when $E_{\rm w}$ first exceeded the initial kinetic energy of the SNR, $E_0 = M_{\rm SNR} v_0^2/2$ ($\sim 10^{51}$ erg), where $t_{\rm acc} = t_{\rm sd} E_0/E_{\rm rot}$. We therefore have

$$\frac{t_{\rm sd}}{t_{\rm acc}} = \frac{E_{\rm rot}}{E_0} = \left(\frac{v_{\rm b}}{v_0}\right)^2 = \left(\frac{R_{\rm b}}{R_{\rm acc}}\right)^{2/3} \approx 100, \tag{4}$$

where $v_{\rm b} \equiv v_{\rm SNR}(t_{\rm sd})$ and $R_{\rm b} \equiv R_{\rm SNR}(t_{\rm sd})$. The dynamics are given by

$$R_{\rm SNR} \approx \begin{cases} v_0 t & t < t_{\rm acc} \\ R_{\rm b}(t/t_{\rm sd})^{3/2} & t > t_{\rm acc}, \end{cases} \tag{5}$$

$$v_{\rm SNR} \approx \begin{cases} v_0 & t < t_{\rm acc} \\ v_{\rm b}(t/t_{\rm sd})^{1/2} & t > t_{\rm acc}. \end{cases} \tag{6}$$

These scalings agree with the results of Reynolds & Chevalier (1984). At $t > t_{\rm acc}$ we have $E_{\rm SNR}/E_{\rm w} = 3\eta_{\rm p}\eta/2$, and conservation of energy implies that $E_0 + E_{\rm w} \approx E_{\rm w} = \eta E_{\rm w} + E_{\rm SNR} = (3\eta_{\rm p}/2 + 1)\eta E_{\rm w}$ or $(3\eta_{\rm p}/2 + 1)\eta = 1$. Our fiducial value of $\eta \approx \xi_{\rm p} = 2/3$ implies $\eta_{\rm p} =$

[1] The total rotational energy of the SMNS is given by $jGM_*^2\,\Omega_*/2c$, where the parameter j measures the stellar angular momentum in units of GM_*^2/c and has values in the range 0.57–0.78 for realistic equations of state (e.g. Cook, Shapiro & Teukolsky 1994; Salgado et al. 1994).

1/3, which is reasonable. We also obtain that $E_{\rm SNR}(t_{\rm sd}) = (3\eta/2)E_{\rm rot} \approx E_{\rm rot}$. For a typical ejected mass, $M_{\rm SNR} \sim 10\,{\rm M}_\odot$, this would imply $v_{\rm b} \sim 0.1c$. Finally, we have

$$R_{\rm b} = \frac{2}{3} v_{\rm b} t_{\rm sd} = 6.3 \times 10^{16} \beta_{\rm b,-1} t_{\rm sd,0}\ {\rm cm}, \tag{7}$$

where we set $v_{\rm b}/c \equiv \beta_{\rm b} = 0.1\beta_{\rm b,-1}$ and $t_{\rm sd} = t_{\rm sd,0}$ yr. To the extent that $v_{\rm b} \propto (E_{\rm rot}/M_{\rm SNR})^{1/2}$ has nearly the same value in all sources, the magnitude of $R_{\rm b}$ is determined by that of $t_{\rm sd}$. In a similar vein, if the energy lost during the SMNS lifetime, $E_{\rm rot} = 10^{53} E_{53}$ erg, is approximately constant from source to source ($E_{53} \sim 1$), then $t_{\rm sd}$ can also be used to parametrize the SMNS wind power: $L_{\rm w} = E_{\rm rot}/t_{\rm sd} = 3.2 \times 10^{45} E_{53}/t_{\rm sd,0}$ erg s^{-1}.

The acceleration of the SNR shell by the lower-density bubble gas would subject it to a Rayleigh–Taylor (RT) instability, which could lead to clumping (Jun 1998). The growth time-scale of the RT instability on a spatial scale R is $t_{\rm RT} \sim (R/\ddot{R})^{1/2}$. The important quantity to estimate in order to see whether the SNR shell can be clumped is the ratio between $t_{\rm RT}$ and the dynamical time-scale $t_{\rm dyn} = (R/\dot{R})$,

$$\frac{t_{\rm RT}}{t_{\rm exp}} = \frac{\dot{R}}{(\ddot{R}R)^{1/2}} = \sqrt{\frac{2E_{\rm SNR}}{\eta_{\rm p}\eta E_{\rm w}}}, \tag{8}$$

where we have used equation (3). This implies $t_{\rm RT}/t_{\rm exp} \approx \sqrt{3}$ during the acceleration ($t_{\rm acc} < t < t_{\rm sd}$). This could produce only moderately strong fragmentation over the dynamical time of the system. However, as the acceleration occurs over ~3 orders of magnitude in radius (see equation 4), the radius doubles itself ~10 times during the course of the SNR acceleration, so that despite the fact that $t_{\rm RT}/t_{\rm exp}$ is of the order of unity, it is feasible that considerable clumpiness may still be caused because of the RT instability. An even stronger fragmentation may occur if the RT instabilities grow on a length-scale $x \sim \alpha R$ smaller than R (i.e. $\alpha < 1$), where in this case $t_{\rm RT}/t_{\rm exp} \approx \sqrt{3\alpha}$.

In order to calculate the emission from the plerion, we use the average quantities of the shocked pulsar wind within the PWB, and neglect their variation with radius. The latter is expected to be more important in the afterglow emission, and is therefore taken into account in Section 6, which discusses the afterglow emission. The post-shock energy density is given by

$$e = \frac{\eta E_{\rm rot}}{V} = \frac{3\eta E_{\rm rot}}{4\pi R_{\rm b}^3}, \tag{9}$$

where $V = (4\pi/3)R_{\rm b}^3$ is the total volume within the PWB, and is approximately equal to the volume occupied by the shocked wind. For an elongated PWB the expression for the volume, V, will be different, but it can directly be plugged into these equations, in place of the spherical expression. The injection rates of electron–positron pairs and of protons at the source are given by

$$\dot{N}_{\rm e,p} = \frac{\xi_{\rm e,p} L_{\rm w}}{\gamma_{\rm w} m_{\rm e,p} c^2}. \tag{10}$$

Hence, the total number of particles within $R_{\rm b}$ at time t is $N_{\rm e,p}(t) = \dot{N}_{\rm e,p} t$, and the number density at $t_{\rm sd}$ is

$$n_{\rm e,p} = \frac{N_{\rm e,p}(t_{\rm sd})}{V} = \frac{\xi_{\rm e,p} e}{\eta \gamma_{\rm w} m_{\rm e,p} c^2} = \frac{3\xi_{\rm e,p} E_{\rm rot}}{4\pi \gamma_{\rm w} m_{\rm e,p} c^2 R_{\rm b}^3}. \tag{11}$$

Fractions $\epsilon_{{\rm b}B}$, $\epsilon_{\rm be}$, $\epsilon_{\rm bp}$ of the post-shock energy density go to the magnetic field, the electrons and the protons, respectively. We expect these fractions to be similar to those in the pulsar wind ($\epsilon_{{\rm b}B} \sim \xi_B \sim \sigma_{\rm w}$, $\epsilon_{\rm be} \sim \xi_{\rm e}$) and use the corresponding fiducial values. Subscripts containing the letter 'b' denote quantities related to the PWB. The electrons will lose energy through synchrotron emission and inverse-Compton (IC) scattering. We study the characteristic features of the plerion emission and investigate the conditions required for the production of the observed iron lines and whether the plerion can be detected by the present instruments. Moreover, an important implication of the plerion emission is that the GRB should explode inside a radiation-rich environment (i.e. the luminous radiation field of the PWB). The external photons are highly Doppler-boosted in the rest frame of the shocked fluid, for both internal and external shocks (that are responsible for the prompt GRB and afterglow emission, respectively), and can act as efficient seed photons for IC scattering (external Comptonization, EC). We study the observational consequences of the EC process, both for the prompt GRB emission and for the afterglow.

Since we use a large number of parameters in the paper, and in order to make it easier to follow all the different parameters, we include a table (Table 1) with the most often used parameters, where we mention the meaning of each parameter and the fiducial value that we use for that parameter.

3 X-RAY LINES IN THE AFTERGLOW

One of the main motivations for the supranova model is that it can naturally explain the detections of iron lines in the X-ray afterglows of several GRBs, both in emission (GRB 970508, Piro et al. 1998; GRB 970828, Yoshida et al. 2001; GRB 000214, Antonelli et al. 2000; GRB 991216, Piro et al. 2000) and in absorption (GRB 990705; Amati et al. 2000). The statistical significance of these detections is at the ~3σ level, with the exception of GRB 991216 where a k-α emission line was detected with a significance of ~4σ. Emission lines of lighter elements (Mg, Si, S, Ar, Ca) have been reported in the X-ray afterglow of GRB 011211, at the level of 3σ (Reeves et al. 2002). This latter detection has been disputed by other authors (Borozdin & Trudolyubov 2003; Rutledge & Sako 2003), and may be said to be controversial. These line features may naturally arise in the context of the supranova model, where an SNR shell is located at a distance of $R \gtrsim 10^{16}$ cm from the location of the GRB explosion (Lazzati et al. 1999; Piro et al. 2000; Böttcher, Fryer & Dermer 2002; Lazzati et al. 2001; Vietri et al. 2001). In this section we explore the condition under which such features may occur within our model, and obtain the relevant constraints on

Table 1. The parameters most often used in the paper, their meaning and fiducial values.

Parameter	Meaning	Fiducial value
$t_{\rm sd}$	Time delay between SN and GRB	1 or $10^{3/2}$ yr
$\gamma_{\rm w}$	Lorentz factor of pulsar wind	$10^{4.5}$
$E_{\rm rot}$	Rotational energy lost by SMNS	10^{53} erg
$M_{\rm SNR}$	The mass of the SNR shell	10 $M_\odot$
η	Fraction of $E_{\rm rot}$ that remains in the PWB	2/3
ξ_B	Fraction of wind energy in magnetic field	10^{-3}
$\xi_{\rm e}$	Fraction of wind energy in $e^\pm$ pairs	1/3
$\xi_{\rm p}$	Fraction of wind energy in protons	2/3
$\beta_{\rm b}$	Velocity of SNR shell at $t_{\rm sd}$ (in units of c)	0.1
$\epsilon_{{\rm b}B}$	Fraction of PWB energy in magnetic field	10^{-3}
$\epsilon_{\rm be}$	Fraction of PWB energy in $e^\pm$ pairs	1/3
a	Fraction of $e^\pm$ energy that is radiated	1
s	Power-law index of $e^\pm$ distribution in PWB	2.2
p	Electron power-law index in the GRB	2.5
Γ	Bulk Lorentz factor of GRB ejecta	$10^{5/2}$
$L_{\rm w}$	Kinetic luminosity of GRB outflow	10^{52} erg s^{-1}
t_v	Variability time of GRB central engine	10 ms
k	$n, e \propto r^{-k}$ in the PWB	0 or 1
ϵ_B	Fraction of AG energy in magnetic field	10^{-3}
$\epsilon_{\rm e}$	Fraction of AG energy in electrons	0.1
$E_{\rm iso}$	Isotropic equivalent energy in AG shock	10^{53} erg
t	Observed time since GRB	1 d

the model parameters. In the following sections we investigate the implications of these constraints on the other observational signatures of the model: the plerion, prompt GRB and afterglow emissions.

We derive constraints on our model parameters using the observational data for GRB 991216, as an example of an afterglow for which iron lines were detected, since this is the most statistically significant detection to date. Similar constraints may be obtained for other afterglows with X-ray features, using similar arguments. The X-ray afterglow of GRB 991216 was observed by *Chandra* from 37 to 40 h after the GRB, and shows an emission line at 3.49 ± 0.06 keV, with a significance of $\sim 4\sigma$. The line flux was $F_{\rm Fe} \sim 1.6 \times 10^{-13}$ erg cm^{-2} s^{-1}, which for a redshift $z = 1.02$ of this burst (Vreeswijk et al. 1999) implies an emission rate $\dot{N}_{\rm Fe} \sim 4 \times 10^{52}$ s^{-1} of line photons, a luminosity of $L_{\rm Fe} \sim 4 \times 10^{44}$ erg s^{-1} and a total energy of $E_{\rm Fe} \sim 3 \times 10^{49}$ erg, assuming the line emission lasted for $t_{\rm Fe} \sim 40/(1+z)$ h in the cosmological rest frame of the GRB (Vietri et al. 2001).

In the simplest version of our model, we assume a spherical geometry, and identify the line-emitting material with the SNR shell, which is located at a radius $R_{\rm b}$. We use the above observations to derive constraints on $R_{\rm b}$, or equivalently, on the time delay between the SN and the GRB events, $t_{\rm sd}$. The value of $R_{\rm b}$ may be constrained by the requirement that the geometrical time delay in the arrival of the photons to the observer, $\sim R_{\rm b}\theta_{\rm rad}^2/2$, should not exceed the total duration of the iron line emission, $t_{\rm Fe}$,

$$R_{\rm b} \lesssim 1.7 \times 10^{18} \left(\frac{t_{\rm Fe}}{20\ {\rm h}}\right)\left(\frac{\theta_{\rm rad}}{0.05}\right)^{-2} {\rm cm}, \quad t_{\rm sd} \lesssim 27 \left(\frac{t_{\rm Fe}}{20\ {\rm h}}\right)\left(\frac{\theta_{\rm rad}}{0.05}\right)^{-2} \beta_{\rm b,-1}^{-1}\ {\rm yr}, \tag{12}$$

where we have identified the opening angle to which the ionizing radiation extends, $\theta_{\rm rad}$, with the jet opening angle, $\theta_j \approx 0.05$ (Frail et al. 2001; Panaitescu & Kumar 2002).

Another constraint may arise from the requirement that $\dot{N}_{\rm Fe} = N_{\rm Fe}/t_{\rm rec} \sim 4 \times 10^{52}$ s^{-1}, where the recombination time is given by $t_{\rm rec} \approx 4 \times 10^9 Z^{-2} T_{\rm e}^{0.6} n_{\rm e}^{-1} = 2.8 \times 10^{10} T_6^{0.6} n_{\rm e}^{-1}$ s, $T_6 = T_{\rm e}/10^6$ K, and we have assumed an electric charge of $Z = 24$ for the iron ions (Lazzati et al. 2001; KG). In order to parametrize the electron number density, $n_{\rm e}$, we need to relate between the width of the SNR shell, $\Delta R_{\rm b}$, and its radius, $R_{\rm b}$. If the SNR shell is efficiently fragmented during its acceleration phase, as a result of the RT instability, then one might expect dense clumps of size $l_{\rm cl} \ll \Delta R_{\rm b}$, spread over a radial interval of $\Delta R_{\rm b}$, that cover a fraction of the order of unity of the total solid angle. This amounts to an effective width for the SNR shell of $\Delta R_{\rm eff} = l_{\rm cl} \ll \Delta R_{\rm b}$, implying $n_{\rm e} = M_{\rm SNR}/4\pi {R_{\rm b}}^2 \Delta R_{\rm eff} m_{\rm p}$ and

$$R_{\rm b} \lesssim 9 \times 10^{16} M_{\rm SNR,1}^{1/3} M_{\rm Fe,-1}^{1/3} \xi_{-3}^{-1/3} T_6^{-1/5}\ {\rm cm}, \quad t_{\rm sd} \lesssim 1.4 M_{\rm SNR,1}^{1/3} M_{\rm Fe,-1}^{1/3} \xi_{-3}^{-1/3} T_6^{-1/5} \beta_{\rm b,-1}^{-1}\ {\rm yr}, \tag{13}$$

where $\xi \equiv \Delta R_{\rm eff}/R_{\rm b} = 10^{-3}\xi_{-3}$ and $M_{\rm Fe} = 0.1 M_{\rm Fe,-1}\ {\rm M}_\odot$ is the mass of the iron in the SNR shell. The SNR shell is compressed during its acceleration, and may attain $\Delta R_{\rm b} \lesssim 0.1 R_{\rm b}$, so that ξ may be as low as $\sim 10^{-3}$.

A final constraint may be derived by considerations related to the total energy budget. The total energy in the line is $E_{\rm Fe} \equiv \varepsilon E_\gamma \sim 3 \times 10^{49}$ erg, where the efficiency ε is the product of the ratio of energies in the ionizing X-ray continuum and the prompt gamma-ray emission, and the energy fraction of the X-ray continuum that goes into the line emission, and is expected to be $\lesssim 0.01$ (Ghisellini et al. 2002). This implies $E_\gamma \gtrsim 3 \times 10^{51}$ erg, which is somewhat in excess of the value $E_\gamma \approx 7 \times 10^{50}$ erg found by Frail et al. (2001). If the optical depth of the iron atoms is $\tau_{\rm Fe} < 1$, then the efficiency is further reduced by a factor of $\tau_{\rm Fe} = M_{\rm Fe}\sigma_{\rm Fe}/4\pi R_{\rm b}^2\, 56 m_{\rm p}$, where $\sigma_{\rm Fe} \approx 2.0 \times 10^{-20}$ cm^2 (Krolik & Kallman 1987). Therefore, we must have $\tau_{\rm Fe} \gtrsim 1$, i.e.

$$R_{\rm b} \lesssim 6\times10^{16} M_{\rm Fe,-1}^{1/2}\ {\rm cm}, \quad t_{\rm sd} \lesssim 0.9 M_{\rm Fe,-1}^{1/2}\beta_{\rm b,-1}^{-1}\ {\rm yr}. \tag{14}$$

We conclude that X-ray line features, such as those observed in the afterglow of several GRBs, may be accommodated in a spherical model only for $t_{\rm sd} \lesssim 1$ yr, $R_{\rm b} \lesssim 10^{17}$ cm. This constraint can be relaxed for an elongated PWB. In this case the iron lines may be produced by the material near the equator, which is at a much smaller radius than the polar radius, enabling the afterglow shock that propagates along the poles to reach a considerably larger radius.

4 THE PLERION EMISSION

In this section we evaluate the luminosity and the spectrum emitted by the plerion. We use the average values of the quantities within the PWB, which were derived in Section 2. As we show below, the electrons are in the fast cooling regime for relevant values of $t_{\rm sd}$, and therefore most of the emission takes place within a small radial interval just behind the wind termination shock, and the various quantities should not vary significantly within this region, and should not be very different from their average values within the PWB.

The magnetic field inside the plerion is

$$B_{\rm b} = \sqrt{8\pi\epsilon_{{\rm b}B}e} \approx 1.3\eta_{2/3}^{1/2}\epsilon_{{\rm b}B,-3}^{1/2}E_{\rm rot,53}^{1/2}\beta_{\rm b,-1}^{-3/2}t_{\rm sd,0}^{-3/2}\ {\rm G}, \tag{15}$$

where $\epsilon_{{\rm b}B,-3} = \epsilon_{{\rm b}B}/10^3$ and $\eta_{2/3} = \eta/(2/3)$. Relativistic electrons/positrons (hereafter simply electrons) are injected into the plerion at the rate $\dot{N}_{\rm e}$ (see equation 10) with a power-law distribution $N(\gamma_{\rm b}) \equiv {\rm d}n/{\rm d}\gamma_{\rm b} \propto \gamma_{\rm b}^{-s}$ in the Lorentz factor (LF) range $\gamma_{{\rm b}m} \lesssim \gamma_{\rm b} \lesssim \gamma_{{\rm b}M}$. The minimum electron LF is given by

$$\gamma_{{\rm b}m} = \left(\frac{s-2}{s-1}\right)\frac{\epsilon_{\rm be}e}{n_{\rm e}m_{\rm e}c^2} \approx 3.5\times10^3\eta_{2/3}\epsilon_{{\rm be},1/3}\xi_{{\rm e},1/3}^{-1}\gamma_{\rm w,4.5}, \tag{16}$$

where $\gamma_{\rm w,4.5} = \gamma_{\rm w}/10^{4.5}$, $\epsilon_{{\rm be},1/3} = \epsilon_{\rm be}/(1/3)$, $\xi_{{\rm e},1/3} = \xi_{\rm e}/(1/3)$ and we use $s = 2.2$ to obtain the numerical values for the rest of the paper. The electrons radiatively cool by the combination of the synchrotron and synchrotron-self-Compton (SSC) process, the time-scales of which are $t_{\rm syn} \sim 6\pi m_{\rm e}c/\sigma_{\rm T}B_{\rm b}^2\gamma_{\rm b}$ and $t_{\rm SC} = t_{\rm syn}/Y_{\rm b}$ and the combined cooling time being $t_{\rm c} = (1/t_{\rm syn} + 1/t_{\rm SC})^{-1} = t_{\rm syn}/(1+Y_{\rm b})$, where

$$Y_{\rm b} \sim \frac{a\epsilon_{\rm be}}{(1+Y_{\rm b})\epsilon_{{\rm b}B}}, \quad Y_{\rm b} \approx \begin{cases} a\epsilon_{\rm be}/\epsilon_{{\rm b}B} & a\epsilon_{\rm be}/\epsilon_{{\rm b}B} \ll 1 \\ \sqrt{a\epsilon_{\rm be}/\epsilon_{{\rm b}B}} & a\epsilon_{\rm be}/\epsilon_{{\rm b}B} \gg 1 \end{cases} \tag{17}$$

(Sari, Narayan & Piran 1996; Panaitescu & Kumar 2000; Sari & Esin 2001)[2] is the Compton y-parameter of the plerion, which is the fractional energy gain of a photon when travelling through the plerion, owing to upscattering by the relativistic electrons and $a \equiv \min[1, (\gamma_{{\rm b}m}/\gamma_{\rm bc})^{s-2}]$ is the fraction of the internal energy in the electrons that is radiated away (Sari & Esin 2001). For our choice of parameters $\epsilon_{{\rm b}B} \ll \epsilon_{\rm be}$ and there is fast cooling so that $a = 1$. This implies $Y_{\rm b} \approx (\epsilon_{\rm be}/\epsilon_{{\rm b}B})^{1/2}$, and we shall use this relation in the following. The maximum LF is set by equating $t_{\rm c}$ with the acceleration time $\sim 2\pi\gamma_{\rm b}m_{\rm e}c/qB_{\rm b}$ (where q is the electric charge of the electron):

$$\gamma_{{\rm b}M} = \sqrt{\frac{3q}{B_{\rm b}\sigma_{\rm T}(1+Y_{\rm b})}} \approx 9.7\times10^6 a^{-1/4}\eta_{2/3}^{-1/4}\epsilon_{{\rm be},1/3}^{-1/4}E_{\rm rot,53}^{-1/4}\beta_{\rm b,-1}^{3/4}t_{\rm sd,0}^{3/4}. \tag{18}$$

The LF of an electron that cools on the adiabatic expansion time $t_{\rm sd}$ (i.e. an electron for which $t_{\rm c} = t_{\rm sd}$) is given by

$$\gamma_{\rm bc} = \frac{6\pi m_{\rm e}c}{(1+Y_{\rm b})B_{\rm b}^2\sigma_{\rm T}t_{\rm sd}} \approx 0.84 a^{-1/2}\eta_{2/3}^{-1}\epsilon_{{\rm be},1/3}^{-1/2}\epsilon_{{\rm b}B,-3}^{-1/2}E_{\rm rot,53}^{-1}\beta_{\rm b,-1}^{3}t_{\rm sd,0}^{2}. \tag{19}$$

For $t_{\rm sd} < t_1$, where

$$t_1 \approx 1.1\eta_{2/3}^{1/2}\epsilon_{{\rm be},1/3}^{1/4}\epsilon_{{\rm b}B,-3}^{1/4}E_{\rm rot,53}^{1/2}\beta_{\rm b,-1}^{-3/2}\ {\rm yr}, \tag{20}$$

the cooling is so fast that equation (19) implies $\gamma_{\rm bc} < 1$. This means that all electrons cool to non-relativistic random velocities within a time $\sim\gamma_{\rm bc}t_{\rm sd}$ and a distance $\sim\gamma_{\rm bc}R_{\rm b}$ behind the termination shock of the pulsar wind. Of course, in this regime $\gamma_{\rm bc} < 1$ no longer corresponds to the physical LF of the electrons.[3] We shall call this regime very fast cooling.

In the case of a non-spherical (elongated) PWB, we can still use the same expressions, if we make the simple substitution described below. We define an effective radius, $R_{\rm eff} \equiv (3V/4\pi)^{1/3}$, so that a sphere of that radius will have the same volume, V, as the non-spherical PWB. Since the volume of the PWB determines its average number density and energy density (which determine the PWB emission), and since we expect the interior of the PWB to be roughly homogeneous (i.e. the local values are not very different from the mean values), then we can reproduce the expressions appropriate for a non-spherical model by simply replacing $R_{\rm b}$ with $R_{\rm eff}$. Since $\beta_{\rm b}$ appears in the various expressions only through $R_{\rm b}$, we may achieve this task most easily by substituting $\beta_{\rm b} = 3R_{\rm eff}/2ct_{\rm sd}$ everywhere. In order to illustrate the effects of a non-spherical geometry, we consider a particular example (which we also consider to be likely) of an elongated PWB with a polar

[2] Sari and Esin pointed out that generally the factor a should be multiplied by the fluid velocity just behind the shock (in the shock frame), which for a relativistic shock with $\epsilon_B \ll 1$, that is relevant for the pulsar wind termination shock, is $\beta = 1/3$. This factor of 1/3 should be divided by the ratio of the radiation flux and the photon energy density times c, which is 1/4 for an isotropic emission in the local rest frame of the emitting fluid. Together this gives a factor of 4/3 which is close to 1, and is therefore neglected.

[3] Formally we obtain $\gamma_{\rm bc} < 1$ because we used the approximation $\beta^2 \approx 1$ in the expression for the total synchrotron power of a single electron, under the assumption (which does not hold here) that the electrons are always relativistic.

radius much larger than the equatorial radius, $R_{\rm p} \gg R_{\rm eq}$, where $R_{\rm p}/2 \lesssim R_{\rm eff} < R_{\rm p}$. If the surface mass density at the poles is sufficiently small, then the velocity of the SNR shell there can become close to c, so that $R_{\rm p} \approx ct_{\rm sd}$. This would imply $\beta_{\rm b} = 3R_{\rm eff}/2ct_{\rm sd} \approx 1$.

4.1 The synchrotron spectrum

The characteristic synchrotron frequency of an electron with LF $\gamma_{\rm b}$ is $\nu_{\rm b} = \gamma_{\rm b}^2 \nu_{\rm b0}$, where $\nu_{\rm b0} = 3qB_{\rm b}/16\, m_{\rm e}c$. The synchrotron frequencies corresponding to $\gamma_{{\rm b}m}$, $\gamma_{{\rm b}M}$ and $\gamma_{\rm bc}$, respectively, are

$$\nu_{\rm bc} \approx 2.9 \times 10^6 (1+z)^{-1} a^{-1} \eta_{2/3}^{-3/2} \epsilon_{{\rm be},1/3}^{-1} \epsilon_{{\rm b}B,-3}^{-1/2} E_{{\rm rot},53}^{-3/2} \beta_{{\rm b},-1}^{9/2} t_{{\rm sd},0}^{5/2}\ {\rm Hz},$$

$$\nu_{{\rm b}m} \approx 5.1 \times 10^{13} (1+z)^{-1} \eta_{2/3}^{5/2} \epsilon_{{\rm be},1/3}^{2} \epsilon_{{\rm b}B,-3}^{1/2} \xi_{{\rm e},1/3}^{-2} E_{{\rm rot},53}^{1/2} \gamma_{{\rm w},4.5}^{2} \beta_{{\rm b},-1}^{-3/2} t_{{\rm sd},0}^{-3/2}\ {\rm Hz},$$

$$\nu_{{\rm b}M} \approx 3.9 \times 10^{20} (1+z)^{-1} a^{-1/2} \epsilon_{{\rm be},1/3}^{-1/2} \epsilon_{{\rm b}B,-3}^{-1/2}\ {\rm Hz}. \tag{21}$$

For $t_{\rm sd} < t_2$ (which is given in equation 35) the synchrotron self-absorption frequency $\nu_{\rm bsa}$ (which is treated below) is above the cooling frequency $\nu_{\rm bc}$, and the synchrotron flux density, F_ν, peaks at $\nu_{\rm bsa}$ and consists of three power-law segments:

$$\frac{F_\nu(t_{\rm sd} < t_2)}{F_{\nu,\rm max}} = \left(\frac{\nu_{\rm bsa}}{\nu_{\rm bc}}\right)^{-1/2} \times \begin{cases} (\nu/\nu_{\rm bsa})^2 & \nu < \nu_{\rm bsa} \\ (\nu/\nu_{\rm bsa})^{-1/2} & \nu_{\rm bsa} < \nu < \nu_{{\rm b}m} \\ (\nu_{{\rm b}m}/\nu_{\rm bsa})^{-1/2} (\nu/\nu_{{\rm b}m})^{-s/2} & \nu_{{\rm b}m} < \nu < \nu_{{\rm b}M}. \end{cases} \tag{22}$$

For time separations between the SN and GRB events, $t_1 < t_{\rm sd} < t_3$, where

$$t_3 \approx 65 \eta_{2/3} \epsilon_{{\rm be},1/3}^{3/4} \epsilon_{{\rm b}B,-3}^{3/4} \xi_{{\rm e},1/3}^{-1/2} E_{{\rm rot},53}^{1/2} \gamma_{{\rm w},4.5}^{1/2} \beta_{{\rm b},-1}^{-3/2}\ {\rm yr}, \tag{23}$$

we have $1 < \gamma_{\rm bc} < \gamma_{{\rm b}m}$ and the bubble is in the (moderately) fast cooling regime. For $t_2 < t_{\rm sd} < t_3$, F_ν peaks at $\nu_{\rm c}$ and is given by

$$\frac{F_\nu(t_2 < t_{\rm sd} < t_3)}{F_{\nu,\rm max}} = \begin{cases} (\nu_{\rm bsa}/\nu_{\rm bc})^{1/3} (\nu/\nu_{\rm bsa})^2 & \nu < \nu_{\rm bsa} \\ (\nu/\nu_{\rm bc})^{1/3} & \nu_{\rm bsa} < \nu < \nu_{\rm bc} \\ (\nu/\nu_{\rm bc})^{-1/2} & \nu_{\rm bc} < \nu < \nu_{{\rm b}m} \\ (\nu_{{\rm b}m}/\nu_{\rm bc})^{-1/2} (\nu/\nu_{{\rm b}m})^{-s/2} & \nu_{{\rm b}m} < \nu < \nu_{{\rm b}M}. \end{cases} \tag{24}$$

For $t_{\rm sd} > t_3$ the bubble is in the slow cooling regime, where the spectrum peaks at $\nu_{{\rm b}m}$ and again consists of four power-law segments:

$$\frac{F_\nu(t_{\rm sd} > t_3)}{F_{\nu,\rm max}} = \begin{cases} (\nu_{\rm bsa}/\nu_{{\rm b}m})^{1/3} (\nu/\nu_{\rm bsa})^2 & \nu < \nu_{\rm bsa} \\ (\nu/\nu_{{\rm b}m})^{1/3} & \nu_{\rm bsa} < \nu < \nu_{{\rm b}m} \\ (\nu/\nu_{{\rm b}m})^{(1-s)/2} & \nu_{{\rm b}m} < \nu < \nu_{\rm bc} \\ (\nu_{\rm bc}/\nu_{{\rm b}m})^{(1-s)/2} (\nu/\nu_{\rm bc})^{-s/2} & \nu_{\rm bc} < \nu < \nu_{{\rm b}M}. \end{cases} \tag{25}$$

The peak synchrotron flux, $F_{\nu,\rm max}$, for either fast or slow cooling, is

$$F_{\nu,\rm max} \approx \frac{\xi_{\rm e} E_{\rm rot} P_{\nu,\rm max}}{\gamma_{\rm w} m_{\rm e} c^2} \frac{(1+z)}{4\pi d_L^2} \approx 42(1+z) \eta_{2/3}^{1/2} \epsilon_{{\rm b}B,-3}^{1/2} \xi_{{\rm e},1/3} E_{{\rm rot},53}^{3/2} \beta_{{\rm b},-1}^{-3/2} t_{{\rm sd},0}^{-3/2} \gamma_{{\rm w},4.5}^{-1} d_{L28}^{-2}\ {\rm mJy}, \tag{26}$$

where $P_{\nu,\rm max} \approx P_{\rm e,syn}/\nu_{\rm syn}$, $P_{\rm e,syn} = 4/3\sigma_{\rm T} c (B_{\rm p}^2/8\pi)\gamma_{\rm e}^2$, $\nu_{\rm syn} = \nu_{\rm b0}\, \gamma_{\rm e}^2$ and $d_L = 10^{28} d_{L28}$ cm is the luminosity distance of the GRB. Synchrotron self-absorption (SSA) will cause a break in the spectrum at a frequency $\nu_{\rm bsa}$ below which[4] $F_\nu \propto \nu^2$. The absorption coefficient is given by

$$\alpha_\nu = -\frac{1}{8\pi m_{\rm e} \nu^2} \int {\rm d}\gamma_{\rm e} P_{\nu,e} \gamma_{\rm e}^2 \frac{\partial}{\partial \gamma_{\rm e}} \left[\frac{N(\gamma_{\rm e})}{\gamma_{\rm e}^2}\right], \tag{27}$$

where

$$P_{\nu,e} \approx P_{\nu,\rm max} \left(\frac{\nu}{\nu_{\rm syn}}\right)^{1/3} \approx \frac{8 m_{\rm e} c^2 B_{\rm p} \sigma_{\rm T}}{9\pi q} \left(\frac{\nu}{\nu_{\rm syn}}\right)^{1/3} \quad \text{for} \quad (\nu < \nu_{\rm syn}) \tag{28}$$

is the spectral emissivity of a single electron.

The electron distribution, $N(\gamma_{\rm e})$, is different for the fast cooling and slow cooling regimes. In the fast cooling case we have

$$N(\gamma_{\rm e}) \approx N_0 \times \begin{cases} \gamma_{\rm e}^{-2} & \max(\gamma_{\rm bc}, 1) < \gamma_{\rm e} < \gamma_{{\rm b}m} \\ \gamma_{{\rm b}m}^{-2} (\gamma_{\rm e}/\gamma_{{\rm b}m})^{-s-1} & \gamma_{{\rm b}m} < \gamma_{\rm e} < \gamma_{{\rm b}M}, \end{cases} \tag{29}$$

with $N_0 = \gamma_{\rm bc} n_{\rm e}$. The local electron distribution depends on the distance behind the shock, l, and the distribution given above is averaged over l. Furthermore, it includes only the relativistic electrons (i.e. for $\gamma_{\rm c} < 1$, most electrons would cool to non-relativistic random Lorentz factors, and are not included in this distribution).

For $\nu < \max(\nu_{\rm bc}, \nu_{\rm b0})$, all the electrons with $\gamma_{\rm e} > \max(\gamma_{\rm c}, 1)$ contribute to the SSA and the absorption coefficient is

$$\alpha_\nu \approx \frac{3 N_0 P_{\nu,\rm max}}{16\pi m_{\rm e} \nu^{5/3} \nu_{\rm b0}^{1/3}} \min(\gamma_{\rm bc}^{-8/3}, 1). \tag{30}$$

[4] For PWBs, this also applies for the fast cooling regime, as opposed to the spectral slope of $F_\nu \propto \nu^{11/8}$ (Granot, Piran & Sari 2000; Granot & Sari 2002) predicted for GRBs (both for the prompt emission and afterglow) since for the PWB the observer faces the back of the shell, i.e. the side further from the shock, where the coolest electrons reside.

If $\max(\nu_{\rm bc}, \nu_{\rm b0}) < \nu < \nu_{{\rm b}m}$ we have

$$\alpha_\nu \approx \frac{3N_0 P_{\nu,\max}}{16\pi m_{\rm e}\nu^{5/3}\nu_{\rm b0}^{1/3}}\left(\frac{16 m_{\rm e} c\nu}{3qB_{\rm b}}\right)^{-4/3}, \tag{31}$$

and, finally, if $\nu > \nu_{{\rm b}m}$ then

$$\alpha_\nu \approx \frac{3N_0 P_{\nu,\max}}{16\pi m_{\rm e}\nu^{5/3}\nu_{\rm b0}^{1/3}}\left(\frac{16 m_{\rm e} c\nu}{3qB_{\rm b}}\right)^{-(s+5/3)/2}\gamma_{{\rm b}m}^{s-1}. \tag{32}$$

In the slow cooling case we have

$$N(\gamma_{\rm e}) \approx N_0 \times \begin{cases} \gamma_{\rm e}^{-s} & \gamma_{{\rm b}m} < \gamma_{\rm e} < \gamma_{\rm bc} \\ \gamma_{\rm bc}^{-s}(\gamma_{\rm e}/\gamma_{\rm bc})^{-s-1} & \gamma_{\rm bc} < \gamma_{\rm e} < \gamma_{{\rm b}M}, \end{cases} \tag{33}$$

with $N_0 = (s-1)\gamma_{{\rm b}m}^{s-1} n_{\rm e}$. The absorption coefficient for $\nu < \nu_{{\rm b}m}$ is given by

$$\alpha_\nu = \frac{4}{(3s+2)}\frac{N_0 P_{\nu,\max}}{8\pi m_{\rm e}\nu^{5/3}\nu_{\rm b0}^{1/3}}\gamma_{{\rm b}m}^{-s-2/3}. \tag{34}$$

The optical depth to SSA is given by $\tau_{\nu,sa} = \alpha_\nu R_{\rm b}\min(\gamma_{\rm bc}, 1)$, and $\nu_{\rm sa}$ is obtained by equating $\tau_{\nu,sa} = 1$. For $t_{\rm sd} < t_2$, where

$$t_2 \approx 12\eta_{2/3}^{3/7}\epsilon_{{\rm be},1/3}^{5/21}\epsilon_{{\rm b}B,-3}^{4/21}\xi_{{\rm e},1/3}^{2/21}E_{{\rm rot},53}^{11/21}\gamma_{{\rm w},4.5}^{-2/21}\beta_{{\rm b},-1}^{-31/21}\ {\rm yr}, \tag{35}$$

we have $\nu_{\rm bsa} > \nu_{\rm bc}$. Since typically $t_1 < t_2 < t_3$, for $t_{\rm sd} < t_2$ we have either very fast cooling or moderately fast cooling and may use equation (31) to derive

$$\nu_{\rm bsa} \approx 1.9\times 10^{10}(1+z)^{-1}a^{-1/6}\epsilon_{{\rm be},1/3}^{-1/6}\epsilon_{{\rm b}B,-3}^{1/6}\xi_{{\rm e},1/3}^{1/3}E_{{\rm rot},53}^{1/3}\gamma_{{\rm w},4.5}^{-1/3}\beta_{{\rm b},-1}^{-2/3}t_{{\rm sd},0}^{-1}\ {\rm Hz}. \tag{36}$$

For $t_2 < t_{\rm sd} < t_3$ we use equation (30) and obtain

$$\nu_{\rm bsa} \approx 1.1\times 10^{13}(1+z)^{-1}a^{1/2}\eta_{2/3}^{6/5}\epsilon_{{\rm be},1/3}^{1/2}\epsilon_{{\rm b}B,-3}^{7/10}\xi_{{\rm e},1/3}^{3/5}E_{{\rm rot},53}^{9/5}\gamma_{{\rm w},4.5}^{-3/5}\beta_{{\rm b},-1}^{-24/5}t_{{\rm sd},0}^{-19/5}\ {\rm Hz}. \tag{37}$$

Since the SSA frequency approaches $\nu_{{\rm b}m}$ only for very large time delays $t_{\rm sd} \gg t_3$, we do not consider the case $\nu_{\rm bsa} > \nu_{{\rm b}m}$. In the slow cooling regime ($t_{\rm sd} > t_3$) we have

$$\nu_{\rm bsa} \approx 2.9\times 10^{9}(1+z)^{-1}\eta_{2/3}^{-4/5}\epsilon_{{\rm b}B,-3}^{1/5}\xi_{{\rm e},1/3}^{8/5}E_{{\rm rot},53}^{4/5}\gamma_{{\rm w},4.5}^{-8/5}\beta_{{\rm b},-1}^{-9/5}t_{{\rm sd},0}^{-9/5}\ {\rm Hz}. \tag{38}$$

4.2 The SSC spectrum

The SSC spectrum has a similar shape to the synchrotron spectrum, and we approximate it as comprising of broken power laws with characteristic frequencies. For the different ranges in $t_{\rm sd}$, it assumes the following forms:

$$\frac{\nu F_\nu^{\rm SC}(t_{\rm sd} < t_2)}{Y_{\rm b}\nu_{{\rm b}m}F_{\nu_{{\rm b}m}}} = \begin{cases} \left(\nu_{\rm bsa}^{\rm SC*}/\nu_{{\rm b}m}^{\rm SC}\right)^{1/2}\left(\nu/\nu_{\rm bsa}^{\rm SC*}\right)^2 & \nu < \nu_{\rm bsa}^{\rm SC*} \\ \left(\nu/\nu_{{\rm b}m}^{\rm SC}\right)^{1/2} & \nu_{\rm bsa}^{\rm SC*} < \nu < \nu_{{\rm b}m}^{\rm SC} \\ \left(\nu/\nu_{{\rm b}m}^{\rm SC}\right)^{(2-s)/2} & \nu > \nu_{{\rm b}m}^{\rm SC}, \end{cases} \tag{39}$$

$$\frac{\nu F_\nu^{\rm SC}(t_2 < t_{\rm sd} < t_3)}{Y_{\rm b}\nu_{{\rm b}m}F_{\nu_{{\rm b}m}}} = \begin{cases} \left(\nu_{\rm bc}^{\rm SC}/\nu_{{\rm b}m}^{\rm SC}\right)^{1/2}\left(\nu_{\rm bsa}^{\rm SC}/\nu_{\rm bc}^{\rm SC}\right)^{4/3}\left(\nu/\nu_{\rm bsa}^{\rm SC}\right)^2 & \nu < \nu_{\rm bsa}^{\rm SC} \\ \left(\nu_{\rm bc}^{\rm SC}/\nu_{{\rm b}m}^{\rm SC}\right)^{1/2}\left(\nu/\nu_{\rm bc}^{\rm SC}\right)^{4/3} & \nu_{\rm bsa}^{\rm SC} < \nu < \nu_{\rm bc}^{\rm SC} \\ \left(\nu/\nu_{{\rm b}m}^{\rm SC}\right)^{1/2} & \nu_{\rm bc}^{\rm SC} < \nu < \nu_{{\rm b}m}^{\rm SC} \\ \left(\nu/\nu_{{\rm b}m}^{\rm SC}\right)^{(2-s)/2} & \nu > \nu_{{\rm b}m}^{\rm SC}, \end{cases} \tag{40}$$

$$\frac{\nu F_\nu^{\rm SC}(t_{\rm sd} > t_3)}{Y_{\rm b}\nu_{\rm bc}F_{\nu_{\rm bc}}} = \begin{cases} \left(\nu_{{\rm b}m}^{\rm SC}/\nu_{\rm bc}^{\rm SC}\right)^{(3-s)/2}\left(\nu_{\rm bsa}^{\rm SC}/\nu_{{\rm b}m}^{\rm SC}\right)^{4/3}\left(\nu/\nu_{\rm bsa}^{\rm SC}\right)^2 & \nu < \nu_{\rm bsa}^{\rm SC} \\ \left(\nu_{{\rm b}m}^{\rm SC}/\nu_{\rm bc}^{\rm SC}\right)^{(3-s)/2}\left(\nu/\nu_{{\rm b}m}^{\rm SC}\right)^{4/3} & \nu_{\rm bsa}^{\rm SC} < \nu < \nu_{{\rm b}m}^{\rm SC} \\ \left(\nu/\nu_{\rm bc}^{\rm SC}\right)^{(3-s)/2} & \nu_{{\rm b}m}^{\rm SC} < \nu < \nu_{\rm bc}^{\rm SC} \\ \left(\nu/\nu_{\rm bc}^{\rm SC}\right)^{(2-s)/2} & \nu > \nu_{\rm bc}^{\rm SC}, \end{cases} \tag{41}$$

where $\nu_{\rm bsa}^{\rm SC*} \equiv \max(1, \gamma_{\rm bc}^2)\nu_{\rm bsa}$, and

$$\nu_{\rm bc}^{\rm SC} = \gamma_{\rm bc}^2\nu_{\rm bc} \approx 2.1\times 10^{6}(1+z)^{-1}a^{-2}\eta_{2/3}^{-7/2}\epsilon_{{\rm be},1/3}^{2}\epsilon_{{\rm b}B,-3}^{-3/2}E_{{\rm rot},53}^{-7/2}\beta_{{\rm b},-1}^{21/2}t_{{\rm sd},0}^{13/2}\ {\rm Hz},$$

$$\nu_{{\rm b}m}^{\rm SC} = \gamma_{{\rm b}m}^2\nu_{{\rm b}m} \approx 6.4\times 10^{20}(1+z)^{-1}\eta_{2/3}^{9/2}\epsilon_{{\rm be},1/3}^{4}\epsilon_{{\rm b}B,-3}^{1/2}\xi_{{\rm e},1/3}^{-4}E_{{\rm rot},53}^{1/2}\gamma_{{\rm w},4.5}^{4}\beta_{{\rm b},-1}^{-3/2}t_{{\rm sd},0}^{-3/2}\ {\rm Hz}, \tag{42}$$

and

$$\nu_{\rm bsa}^{\rm SC} = \begin{cases} \gamma_{\rm bc}^2 \nu_{\rm bsa} \approx 1.4 \times 10^{10} (1+z)^{-1} a^{-7/6} \eta_{2/3}^{-2} \epsilon_{{\rm be},1/3}^{-7/6} \epsilon_{{\rm b}B,-3}^{-5/6} \xi_{{\rm e},1/3}^{1/3} E_{{\rm rot},53}^{-5/3} \gamma_{{\rm w},4.5}^{-1/3} \beta_{{\rm b},-1}^{16/3} t_{{\rm sd},0}^{3}\ {\rm Hz} & t_1 < t_{\rm sd} < t_2 \\ \gamma_{\rm bc}^2 \nu_{\rm bsa} \approx 8.0 \times 10^{12} (1+z)^{-1} a^{-1/2} \eta_{2/3}^{-4/5} \epsilon_{{\rm be},1/3}^{-1/5} \epsilon_{{\rm b}B,-3}^{-3/10} \xi_{{\rm e},1/3}^{3/5} E_{{\rm rot},53}^{-1/5} \gamma_{{\rm w},4.5}^{-3/5} \beta_{{\rm b},-1}^{6/5} t_{{\rm sd},0}^{1/5}\ {\rm Hz} & t_2 < t_{\rm sd} < t_3 \\ \gamma_{{\rm b}m}^2 \nu_{\rm bsa} \approx 3.6 \times 10^{16} (1+z)^{-1} \eta_{2/3}^{6/5} \epsilon_{{\rm be},1/3} \epsilon_{{\rm b}B,-3}^{1/5} \xi_{{\rm e},1/3}^{-2/5} E_{{\rm rot},53}^{4/5} \gamma_{{\rm w},4.5}^{2/5} \beta_{{\rm b},-1}^{-9/5} t_{{\rm sd},0}^{-9/5}\ {\rm Hz} & t_{\rm sd} > t_3. \end{cases} \tag{43}$$

The peak of $\nu F_\nu^{\rm SC}$ is simply $Y_{\rm b}$ times the peak of the synchrotron νF_ν, which for fast cooling is given by

$$\nu_{{\rm b}m} F_{\nu_{{\rm b}m}} = \nu_{{\rm b}m} F_{\nu,\max} \sqrt{\frac{\nu_{\rm bc}}{\nu_{{\rm b}m}}} \approx 5.1 \times 10^{-15} a^{-1/2} \eta_{2/3} \epsilon_{{\rm be},1/3}^{1/2} \epsilon_{{\rm b}B,-3}^{1/2} E_{{\rm rot},53} t_{{\rm sd},0}^{-1}\, d_{L28}^{-2}, \tag{44}$$

and for slow cooling is given by this expression multiplied by the factor of a.

4.3 The Klein–Nishina effect

When the energy of the seed (synchrotron) photon in the rest frame of the scattering electron exceeds the electrons rest energy, $\gamma_{\rm e}\, h\nu^{\rm syn} \gtrsim m_{\rm e}c^2$, then we move from the Thomson limit to the Klein–Nishina (KN) regime, where there is a reduction in the scattering cross-section and the electron recoil becomes important. The corresponding frequencies where the KN limit is reached for the seed synchrotron photon and upscattered (SC) photon are given by

$$\frac{\nu_{\rm KN}^{\rm SC}}{\gamma_{\rm e}} = \gamma_{\rm e} \nu_{\rm KN}^{\rm syn} = \nu_{{\rm KN},0} \equiv \frac{m_{\rm e}c^2}{h} = \frac{c}{\lambda_{\rm c}} = 1.23 \times 10^{20}\ {\rm Hz}, \tag{45}$$

where $\lambda_{\rm c}$ is the Compton wavelength. As the energy increase of the photon arising from the scattering cannot exceed that of the electron, the photon energy of $h\nu_{\rm KN}^{\rm SC} = \gamma_{\rm e} m_{\rm e} c^2$ sets the natural upper limit to the frequency of photons that are upscattered by electrons with an LF $\gamma_{\rm e}$. Typically, either the fractional energy gain in successive scatterings is $Y \sim \tau_{\rm T}\gamma_{\rm e}^2 \ll 1$, or the KN limit is reached for the second scattering, $\gamma_{\rm e}^3 h\nu^{\rm syn} \gtrsim m_{\rm e}c^2$, thus allowing us to ignore multiple scatterings.

In KN effects typically become important only at $\nu^{\rm SC} > \max\,(\nu_{\rm bsa}^{\rm SC}, \nu_{\rm bc}^{\rm SC})$ in the fast cooling regime, or at $\nu > \nu_{{\rm b}m}^{\rm SC}$ in the slow cooling regime. We therefore restrict our discussion to these frequency ranges of the SSC spectrum. Within this frequency range, the SSC flux density at a given frequency consists of roughly equal contributions from seed synchrotron photons that extend over a finite range of frequencies, that are upscattered by electrons within a finite range of LFs $\gamma_{\rm b}$, so that $\gamma_{\rm b}^2 \nu^{\rm syn} = \nu^{\rm SC} =$ constant. For this reason, a significant change in the SSC flux at a certain frequency $\nu^{\rm SC}$, arising from KN effects, will occur only when all the electrons that contribute significantly to this frequency reach the KN limit. Since $\nu_{\rm KN}^{\rm SC}(\gamma_{\rm b}) \propto \gamma_{\rm b}$, this occurs when the electron with the maximal $\gamma_{\rm b}$ that still contributes significantly to $\nu^{\rm SC}$, $\gamma_{\max}(\nu^{\rm SC})$, reaches the KN limit. For fast cooling

$$\gamma_{\max}(\nu) = \begin{cases} \sqrt{\nu/\nu_{\rm bp}} & \gamma_{\rm bc}^2 \nu_{\rm bp} < \nu < \gamma_{{\rm b}m}^2 \nu_{\rm bp} \\ \gamma_{{\rm b}m} & \gamma_{{\rm b}m}^2 \nu_{\rm bp} < \nu < \nu_{{\rm b}m}^{\rm SC} \\ \sqrt{\nu/\nu_{{\rm b}m}} & \nu_{{\rm b}m}^{\rm SC} < \nu < \gamma_{{\rm b}M}^2 \nu_{{\rm b}m} \\ \gamma_{{\rm b}M} & \nu > \gamma_{{\rm b}M}^2 \nu_{{\rm b}m}, \end{cases} \tag{46}$$

where $\nu_{\rm bp} \equiv \max\,(\nu_{\rm bsa}\,, \nu_{\rm bc})$, while for slow cooling

$$\gamma_{\max}(\nu) = \begin{cases} \sqrt{\nu/\nu_{{\rm b}m}} & \nu_{{\rm b}m}^{\rm SC} < \nu < \gamma_{\rm bc}^2 \nu_{{\rm b}m} \\ \gamma_{\rm bc} & \gamma_{\rm bc}^2 \nu_{{\rm b}m} < \nu < \nu_{\rm bc}^{\rm SC} \\ \sqrt{\nu/\nu_{\rm bc}} & \nu_{\rm bc}^{\rm SC} < \nu < \gamma_{{\rm b}M}^2 \nu_{\rm bc} \\ \gamma_{{\rm b}M} & \nu > \gamma_{{\rm b}M}^2 \nu_{\rm bc}, \end{cases} \tag{47}$$

where $\nu_{\rm bsa} < \nu_{{\rm b}m}$. The KN effects become important at the frequency $\nu_{kN,1}^{\rm SC}$ that satisfies[5] $\nu = \gamma_{\max}\,(\nu)\nu_{{\rm KN},0}$. For fast cooling

$$\nu_{kN,1}^{\rm SC} = \begin{cases} \nu_{{\rm KN},0}^2/\nu_{\rm bp} & \gamma_{\rm bc}^2 \nu_{\rm bp} < \nu_{kN,1}^{\rm SC} < \gamma_{{\rm b}m}^2 \nu_{\rm bp} \\ \gamma_{{\rm b}m} \nu_{{\rm KN},0} & \gamma_{{\rm b}m}^2 \nu_{\rm bp} < \nu_{kN,1}^{\rm SC} < \nu_{{\rm b}m}^{\rm SC} \\ \nu_{{\rm KN},0}^2/\nu_{{\rm b}m} & \nu_{{\rm b}m}^{\rm SC} < \nu_{kN,1}^{\rm SC} < \gamma_{{\rm b}M}^2 \nu_{{\rm b}m} \\ \gamma_{{\rm b}M} \nu_{{\rm KN},0} & \nu_{kN,1}^{\rm SC} > \gamma_{{\rm b}M}^2 \nu_{{\rm b}m}, \end{cases} \tag{48}$$

while for slow cooling

$$\nu_{kN,1}^{\rm SC} = \begin{cases} \nu_{{\rm KN},0}^2/\nu_{{\rm b}m} & \nu_{{\rm b}m}^{\rm SC} < \nu_{kN,1}^{\rm SC} < \gamma_{\rm bc}^2 \nu_{{\rm b}m} \\ \gamma_{\rm bc} \nu_{{\rm KN},0} & \gamma_{\rm bc}^2 \nu_{{\rm b}m} < \nu_{kN,1}^{\rm SC} < \nu_{\rm bc}^{\rm SC} \\ \nu_{{\rm KN},0}^2/\nu_{\rm bc} & \nu_{\rm bc}^{\rm SC} < \nu_{kN,1}^{\rm SC} < \gamma_{{\rm b}M}^2 \nu_{\rm bc} \\ \gamma_{{\rm b}M} \nu_{{\rm KN},0} & \nu_{kN,1}^{\rm SC} > \gamma_{{\rm b}M}^2 \nu_{\rm bc}. \end{cases} \tag{49}$$

[5] From equations (46) and (47) it is evident that there is always exactly one solution to this equation, while the explicit form of this solution depends on the frequency range in which it is obtained.

At $\nu < \nu_{kN,1}^{\rm SC}$ KN effects are unimportant and the SSC spectrum is given by equations (39)–(41). At $\nu > \nu_{kN,1}^{\rm SC}$ KN effects become important. In order to calculate F_ν in this range we first need to estimate the scattering optical depth $\tau_{\rm e}(\gamma_{\rm b})$ of electrons with LF $\gamma_{\rm e} \sim \gamma_{\rm b}$, which is of the same order as the total optical depth of electrons with $\gamma_{\rm e} > \gamma_{\rm b}$:

$$\tau_{\rm e}(\gamma_{\rm b}) \approx \sigma_{\rm T} R_{\rm b} \int_{\gamma_{\rm b}}^{\gamma_{{\rm b}M}} {\rm d}\gamma_{\rm e} N(\gamma_{\rm e}), \tag{50}$$

where $N(\gamma_{\rm e})$ is given in equations (29) and (33) for fast cooling and for slow cooling, respectively. For fast cooling we obtain

$$\tau_{\rm e}(\gamma_{\rm e}) \approx \tau_{\rm T} \times \begin{cases} \gamma_{\rm bc}/\gamma_{\rm e} & \gamma_{\rm bc} < \gamma_{\rm e} < \gamma_{{\rm b}m} \\ \gamma_{\rm bc}\gamma_{{\rm b}m}^{s-1}\gamma_{\rm e}^{-s} & \gamma_{{\rm b}m} < \gamma_{\rm e} < \gamma_{{\rm b}M}, \end{cases} \tag{51}$$

while for slow cooling

$$\tau_{\rm e}(\gamma_{\rm e}) \approx \tau_{\rm T} \times \begin{cases} (\gamma_{\rm e}/\gamma_{{\rm b}m})^{1-s} & \gamma_{{\rm b}m} < \gamma_{\rm e} < \gamma_{\rm bc} \\ \gamma_{\rm bc}\gamma_{{\rm b}m}^{s-1}\gamma_{\rm e}^{-s} & \gamma_{\rm bc} < \gamma_{\rm e} < \gamma_{{\rm b}M}. \end{cases} \tag{52}$$

At $\nu > \nu_{kN,1}^{\rm SC}$ the SSC flux density is dominated by the contribution from electrons with $\nu_{\rm KN}^{\rm SC}(\gamma_{\rm b}) \sim \nu$ and is given by

$$F_\nu^{\rm SC} \approx \tau_{\rm e}(\gamma_{\rm e} = \nu/\nu_{\rm KN,0}) F^{\rm syn}_{\nu_{\rm KN,0}^2/\nu}. \tag{53}$$

The frequency dependence arising from the first term on the right-hand side of equation (53) is just the $\gamma_{\rm e}$ dependence of $\tau_{\rm e}(\gamma_{\rm e})$ (which appears explicitly in equations 51 and 52), while the second term introduces a frequency dependence of $\nu^{-\beta}$ where $F_\nu^{\rm syn} \propto \nu^\beta$ at $\nu^{\rm syn} = \nu_{\rm KN,0}^2/\nu^{\rm SC}$.

In all cases the largest frequency that the SSC spectrum reaches is $\min[\nu_{\rm KN}^{\rm SC}(\gamma_{{\rm b}M}), \gamma_{{\rm b}M}^2\nu_{{\rm b}M}]$. For $\nu_{\rm KN}^{\rm SC}(\gamma_{{\rm b}M}) > \gamma_{{\rm b}M}^2\nu_{{\rm b}M}$ the SSC spectrum is given by equations (39)–(41), with no changes. For $\gamma_{{\rm b}M}^2 \max(\nu_{{\rm b}m}, \nu_{\rm bc}) < \nu_{\rm KN}^{\rm SC}(\gamma_{{\rm b}M}) < \gamma_{{\rm b}M}^2\nu_{{\rm b}M}$, the SSC spectrum is the same as in equations (39)–(41) up to $\nu_{\rm KN}^{\rm SC}(\gamma_{{\rm b}M})$, where it ends sharply [note that $\nu_{\rm KN}^{\rm SC}(\gamma_{{\rm b}M}) = \nu_{\rm KN,1}^{\rm SC}$ in this region].

For fast cooling with $\gamma_{{\rm b}m}^2\nu_{\rm bp} < \nu_{\rm KN,1}^{\rm SC} < \gamma_{{\rm b}M}^2\nu_{{\rm b}m}$ we have $F_\nu^{\rm SC} \propto \nu^{-\beta-s}$ for $\nu_{\rm KN,1}^{\rm SC} < \nu < \nu_{\rm KN}^{\rm SC}(\gamma_{{\rm b}M})$, and the spectrum ends at $\nu_{\rm KN}^{\rm SC}(\gamma_{{\rm b}M})$. Immediately above $\nu_{\rm KN,1}^{\rm SC}$ we have $\beta = -1/2$ while β might change to 1/3 (for $\nu_{\rm bc} > \nu_{\rm bsa}$) or 2 (for $\nu_{\rm bc} < \nu_{\rm bsa}$) at a higher frequency, $\nu_{\rm KN,0}^2/\nu_{\rm bp}$, producing a spectral break at this frequency, if $\nu_{\rm KN,0}^2/\nu_{\rm bp} < \nu_{\rm KN}^{\rm SC}(\gamma_{{\rm b}M})$ [i.e. if $\gamma_{{\rm b}M}^2\nu_{\rm bp} > \nu_{\rm KN}^{\rm SC}(\gamma_{{\rm b}M})$]. For fast cooling with $\gamma_{\rm bc}^2\nu_{\rm bp} < \nu_{\rm KN,1}^{\rm SC} < \gamma_{{\rm b}m}^2\nu_{\rm bp}$ we have $F_\nu^{\rm SC} \propto \nu^{-\beta-1}$ for $\nu_{\rm KN,1}^{\rm SC} < \nu < \nu_{\rm KN}^{\rm SC}(\gamma_{{\rm b}m})$, and $F_\nu^{\rm SC} \propto \nu^{-\beta-s}$ for $\nu_{\rm KN}^{\rm SC}(\gamma_{{\rm b}m}) < \nu < \nu_{\rm KN}^{\rm SC}(\gamma_{{\rm b}M})$, where for $\nu_{\rm bsa} > \nu_{\rm bc}$ we have $\beta = 2$, while for $\nu_{\rm bc} > \nu_{\rm bsa}$ we have $\beta = 1/3$ immediately above $\nu_{\rm KN,1}^{\rm SC}$, which may change to $\beta = 2$ at $\nu_{\rm KN,0}^2/\nu_{\rm bsa}$ if $\nu_{\rm KN,0}^2/\nu_{\rm bsa} < \nu_{\rm KN}^{\rm SC}(\gamma_{{\rm b}M})$.

For slow cooling with $\gamma_{\rm bc}^2\nu_{{\rm b}m} < \nu_{\rm KN,1}^{\rm SC} < \gamma_{{\rm b}M}^2\nu_{\rm bc}$ we have $F_\nu^{\rm SC} \propto \nu^{-\beta-s}$ for $\nu_{\rm KN,1}^{\rm SC} < \nu < \nu_{\rm KN}^{\rm SC}(\gamma_{{\rm b}M})$, and the spectrum ends at $\nu_{\rm KN}^{\rm SC}(\gamma_{{\rm b}M})$. Immediately above $\nu_{\rm KN,1}^{\rm SC}$ we have $\beta = (1-s)/2$, while β might change to 1/3 at a higher frequency, $\nu_{\rm KN,0}^2/\nu_{{\rm b}m}$, producing a spectral break at this frequency, if $\nu_{\rm KN,0}^2/\nu_{{\rm b}m} < \nu_{\rm KN}^{\rm SC}(\gamma_{{\rm b}M})$. For slow cooling with $\gamma_{\rm bc}^{\rm SC} < \nu_{\rm KN,1}^{\rm SC} < \gamma_{\rm bc}^2\nu_{{\rm b}m}$ we have $F_\nu^{\rm SC} \propto \nu^{1-s-\beta}$ for $\nu_{\rm KN,1}^{\rm SC} < \nu < \nu_{\rm KN}^{\rm SC}(\gamma_{\rm bc})$, and $F_\nu^{\rm SC} \propto \nu^{-s-\beta}$ for $\nu_{\rm KN}^{\rm SC}(\gamma_{\rm bc}) < \nu < \nu_{\rm KN}^{\rm SC}(\gamma_{{\rm b}M})$, where $\beta = 1/3$ immediately above $\nu_{\rm KN,1}^{\rm SC}$, and may change to $\beta = 2$ at $\nu_{\rm KN,0}^2/\nu_{\rm bsa}$ if $\nu_{\rm KN,0}^2/\nu_{\rm bsa} < \nu_{\rm KN}^{\rm SC}(\gamma_{{\rm b}M})$.

4.4 Opacity to pair production

High-energy photons emitted in the PWB, either by the plerion itself or by the prompt GRB or afterglow that occur inside the PWB, may interact with lower-energy photons of the strong radiation field of the plerion to create $e^\pm$ pairs. For sufficiently high photon energies, the optical depth to this process, $\tau_{\gamma\gamma}$, may exceed unity, so that they could not escape and reach the observer. We now calculate the photon energy ϵ (in units of $m_{\rm e}c^2$) for which $\tau_{\gamma\gamma}(\epsilon) = 1$. This sets the maximal photon energy that will not be affected by this process.

The radiation field of the plerion is roughly homogeneous and isotropic within the largest radius where the radiation is emitted, which we parametrize as $fR_{\rm b}$. For a fast cooling PWB ($t_{\rm sd} \ll t_3 \sim 65$ yr), the radiation is emitted within a thin layer behind the wind termination shock, at the radius $R_{\rm s}$, so that $f = R_{\rm s}/R_{\rm b}$. For an adiabatic bubble, such as the one considered here, the value of this ratio ranges between 0.2 and 0.5 (KG). For a slow cooling PWB ($t_{\rm sd} > t_3 \sim 65$ yr) the radiation is emitted from the whole volume of the PWB, and $f = 1$. The internal shocks that produce the prompt GRB emission take place at a radius smaller than $fR_{\rm b}$, and the energy density of the plerion radiation field is $U_{\rm ph} \approx a\xi_{\rm e}E_{\rm rot}/t_{\rm sd}2\pi(fR_{\rm b})^2c$. However, the relevant target photons for pair production with high-energy photons are the synchrotron photons, since the synchrotron component is dominant at low energies. Therefore, we should use the energy density of the synchrotron photons, $U_{\rm syn} = U_{\rm ph}/(1+Y_{\rm b})$. As we shall see in Section 6.3, the afterglow emission typically occurs at $R > fR_{\rm b}$, where the radiation field is not homogeneous, but rather drops as $U_{\rm ph} \propto R^{-2}$, and is not isotropic, causing a smaller typical angle between the trajectories of the two photons that could possibly produce an $e^\pm$ pair. Both effects reduce $\tau_{\gamma\gamma}$ for the afterglow emission, compared with that for the prompt GRB or the plerion emission itself, which we calculate below.

The number density of synchrotron photons, n_ϵ, per unit dimensionless photon energy ϵ, may be obtained from the shape of the synchrotron spectrum, and its normalization is

$$\frac{a\xi_{\rm e}E_{\rm rot}}{ct_{\rm sd}2\pi(fR_{\rm b})^2(1+Y_{\rm b})} = U_{\rm syn} = m_{\rm e}c^2 \int {\rm d}\epsilon n_\epsilon \epsilon = g m_{\rm e}c^2 \epsilon_{{\rm b}m}^2 n_{\epsilon_{{\rm b}m}}, \tag{54}$$

where $U_{\rm ph}$ is the photon energy density of the plerion and $g = 2(s-1)/(s-2)$. The optical depth to pair production is given by

$$\tau_{\gamma\gamma}(\epsilon) \approx \sigma_{\rm T} fR_{\rm b}\epsilon^{-1}n_{1/\epsilon} = \sigma_{\rm T} fR_{\rm b}\frac{U_{\rm syn}}{gm_{\rm e}c^2}\epsilon_{{\rm b}m}^{(s-2)/2}\epsilon^{s/2}, \tag{55}$$

and $\tau_{\gamma\gamma}(\epsilon) = 1$ is satisfied for

$$h\nu_{\gamma\gamma} = \frac{\epsilon m_e c^2}{(1+z)} \approx \frac{2.4\ \mathrm{GeV}}{(1+z)} \left(\frac{f_{1/3}}{\sqrt{a}}\right)^{10/11} \eta_{2/3}^{-5/22} \epsilon_{\mathrm{be},1/3}^{3/11} \epsilon_{\mathrm{b}B,-3}^{-1/2} \xi_{\mathrm{e},1/3}^{-8/11} E_{\mathrm{rot},53}^{-21/22} \gamma_{\mathrm{w},4.5}^{-2/11} \beta_{\mathrm{b},-1}^{23/22} t_{\mathrm{sd},0}^{43/22}, \tag{56}$$

where $f_{1/3} = f/(1/3)$. It can be seen from equation (56) that opacity to pair production becomes important only at very high photon energies, and is larger for smaller t_{sd}.

For an elongated PWB, the radiation field can generally have a rather different structure, resulting in a different expression for $\nu_{\gamma\gamma}$. However, one can imagine a simple scenario where the structure of the radiation field is similar to the spherical case, and equation (56) is still applicable with simple substitutions. This can occur if the PWB cools rapidly and most of the radiation is emitted just behind the wind termination shock, and the latter is roughly spherical, with a radius, R_{s}, similar to the equatorial radius, R_{eq}. In this case we should make the usual substitution $\beta_{\mathrm{b}} = 3R_{\mathrm{eff}}/2ct_{\mathrm{sd}}$ and $f = R_{\mathrm{s}}/R_{\mathrm{eff}} \sim R_{\mathrm{eq}}/R_{\mathrm{eff}}$. For example, with $\beta_{\mathrm{b}} \approx 1$ and $R_{\mathrm{eq}}/R_{\mathrm{eff}} \sim 0.1$ this would increase $\nu_{\gamma\gamma}$ by a factor of $\sim$3.

4.5 Prospects for direct detection

An important prediction of this model is a strong radiation field within the PWB. We now examine the possibility of directly observing the radiation emanating from the PWB during the time between the SN and the GRB events. For time separations t_{sd} smaller than

$$t_\tau = 0.4 \left(\frac{M_{\mathrm{SNR}}}{10\ \mathrm{M}_\odot}\right)^{1/2} \beta_{\mathrm{b},-1}^{-1}\ \mathrm{yr}, \tag{57}$$

the SNR shell has a Thomson optical depth larger than unity, and would therefore obscure the radiation emitted within the PWB. For $t_{\mathrm{sd}} < t_\tau$ the emission owing to the radioactive decay of Ni and Co in the SNR shell, might be observed, as in a regular supernova. However, even at the peak of the supernova emission, it will be hard to detect at a cosmological distance. This difficulty is also present in ongoing searches for high-redshift supernovae, where as in our case, random patches of the sky need to be searched, as there is no prompt GRB and afterglow emission to tell us where and when to look.

If there is considerable clumping of the SNR shell before this time, then equation (57) gives the time when the average optical depth of the SNR equals 1, while for regions of the shell with a less than average density the optical depth can drop below unity at a somewhat earlier time. This constraint may also be eased if the geometry of the PWB is not spherical (an elongated PWB), and the mean density of the SNR shell is significantly smaller near the poles compared with near the equator, and our line of sight is near one of the poles (as is required in order to see the prompt γ-ray emission from a jetted GRB).

Once the SNR shell becomes optically thin, the PWB radiation may be detected if the flux that arrives at the observer is sufficiently large. For simplicity, we calculate the flux at the time of the GRB explosion, t_{sd} after the supernova event, since the relevant quantities scale as power laws with the time t after the supernova, and the system spends most of its (logarithmic) time near $t = t_{\mathrm{sd}}$. For concreteness, we consider the observed flux in the radio, optical and X-ray bands, for a typical frequency in each of these frequency ranges: $\nu_{\mathrm{rad}} = 5 \times 10^9$ Hz, $\nu_{\mathrm{op}} = 5 \times 10^{14}$ Hz and $\nu_{\mathrm{X}} = 10^{18}$ Hz.

For the radio band we have $\nu_{\mathrm{rad}} < \nu_{\mathrm{bsa}}$ for $t_{\mathrm{sd}} < t_{\mathrm{sa,rad}}$, $\nu_{\mathrm{bsa}} < \nu_{\mathrm{rad}} < \nu_{\mathrm{bc}}$ for $t_{\mathrm{sa,rad}} < t_{\mathrm{sd}} < t_{\mathrm{c,rad}}$ and $\nu_{\mathrm{bc}} < \nu_{\mathrm{rad}} < \nu_{\mathrm{b}m}$ for $t_{\mathrm{sd}} > t_{\mathrm{c,rad}}$, where

$$t_{\mathrm{sa,rad}} = 3.9(1+z)^{-1} \epsilon_{\mathrm{be},1/3}^{-1/6} \epsilon_{\mathrm{b}B,-3}^{1/6} \xi_{\mathrm{e},1/3}^{1/3} E_{\mathrm{rot},53}^{1/3} \gamma_{\mathrm{w},4.5}^{-1/3} \beta_{\mathrm{b},-1}^{-2/3} \nu_{9.7}^{-1}\ \mathrm{yr}, \tag{58}$$

$$t_{\mathrm{c,rad}} = 20(1+z)^{2/5} \eta_{2/3}^{3/5} \epsilon_{\mathrm{be},1/3}^{2/5} \epsilon_{\mathrm{b}B,-3}^{1/5} E_{\mathrm{rot},53}^{3/5} \beta_{\mathrm{b},-1}^{-9/5} \nu_{14.7}^{2/5}\ \mathrm{yr}, \tag{59}$$

and

$$F_\nu^{\mathrm{syn}} = \begin{cases} 34\ \mu\mathrm{Jy}(1+z)^3 \eta_{2/3}^{-1/4} \epsilon_{\mathrm{be},1/3}^{-1/12} \epsilon_{\mathrm{b}B,-3}^{-1/6} \xi_{\mathrm{e},1/3}^{1/6} E_{\mathrm{rot},53}^{-1/12} \gamma_{\mathrm{w},4.5}^{-1/6} \beta_{\mathrm{b},-1}^{29/12} t_{\mathrm{sd},0}^{9/4} \nu_{9.7}^2 d_{L28}^{-2} & t_{\mathrm{sd}} < t_{\mathrm{sa,rad}} \\ 1.0\ \mathrm{mJy}(1+z)^{1/2} \eta_{2/3}^{-1/4} \epsilon_{\mathrm{be},1/3}^{-1/2} \epsilon_{\mathrm{b}B,-3}^{1/4} \xi_{\mathrm{e},1/3} E_{\mathrm{rot},53}^{3/4} \gamma_{\mathrm{w},4.5}^{-1} \beta_{\mathrm{b},-1}^{3/4} t_{\mathrm{sd},0}^{-1/4} \nu_{9.7}^{-1/2} d_{L28}^{-2} & t_{\mathrm{sa,rad}} < t_{\mathrm{sd}} < t_{\mathrm{c,rad}} \\ 0.50\ \mathrm{Jy}(1+z)^{4/3} \eta_{2/3} \epsilon_{\mathrm{be},1/3}^{1/3} \epsilon_{\mathrm{b}B,-3}^{2/3} \xi_{\mathrm{e},1/3} E_{\mathrm{rot},53}^2 \gamma_{\mathrm{w},4.5}^{-1} \beta_{\mathrm{b},-1}^{-3} t_{\mathrm{sd},0}^{-7/3} \nu_{9.7}^{1/3} d_{L28}^{-2} & t_{\mathrm{sd}} > t_{\mathrm{c,rad}}. \end{cases} \tag{60}$$

For $t_{\mathrm{sd}} < t_{m,\mathrm{op}}$ we have $\nu_{\mathrm{op}} < \nu_{\mathrm{b}m}$, while for $t_{\mathrm{sd}} > t_{m,\mathrm{op}}$, the ordering is reversed $\nu_{\mathrm{op}} > \nu_{\mathrm{b}m}$, where $t_{m,\mathrm{op}}$ is given by

$$t_{m,\mathrm{op}} = 0.22(1+z)^{-2/3} \eta_{2/3}^{5/3} \epsilon_{\mathrm{be},1/3}^{4/3} \epsilon_{\mathrm{b}B,-3}^{1/3} \xi_{\mathrm{e},1/3}^{-4/3} E_{\mathrm{rot},53}^{1/3} \gamma_{\mathrm{w},4.5}^{4/3} \beta_{\mathrm{b},-1}^{-1} \nu_{14.7}^{-2/3}\ \mathrm{yr}. \tag{61}$$

The optical flux is dominated by synchrotron emission and is given by

$$F_\nu^{\mathrm{syn}} = \begin{cases} 3.1\ \mu\mathrm{Jy}(1+z)^{1/2} \eta_{2/3}^{-1/4} \epsilon_{\mathrm{be},1/3}^{-1/2} \epsilon_{\mathrm{b}B,-3}^{1/4} \xi_{\mathrm{e},1/3} E_{\mathrm{rot},53}^{3/4} \gamma_{\mathrm{w},4.5}^{-1} \beta_{\mathrm{b},-1}^{3/4} t_{\mathrm{sd},0}^{-1/4} \nu_{14.7}^{-1/2} d_{L28}^{-2} & t_{\mathrm{sd}} < t_{m,\mathrm{op}} \\ 0.82\ \mu\mathrm{Jy}(1+z)^{-1/10} \eta_{2/3}^{5/4} \epsilon_{\mathrm{be},1/3}^{7/10} \epsilon_{\mathrm{b}B,-3}^{11/20} \xi_{\mathrm{e},1/3}^{-1/5} E_{\mathrm{rot},53}^{21/20} \gamma_{\mathrm{w},4.5}^{1/5} \beta_{\mathrm{b},-1}^{-3/20} t_{\mathrm{sd},0}^{-23/20} \nu_{14.7}^{-11/10} d_{L28}^{-2} & t_{\mathrm{sd}} > t_{m,\mathrm{op}}. \end{cases} \tag{62}$$

The X-ray is typically above $\nu_{\mathrm{b}m}$, and for the synchrotron emission we have

$$\nu F_\nu^{\mathrm{syn}} = 1.9 \times 10^{-15}(1+z)^{-1/10} \eta_{2/3}^{5/4} \epsilon_{\mathrm{be},1/3}^{7/10} \epsilon_{\mathrm{b}B,-3}^{11/20} \xi_{\mathrm{e},1/3}^{-1/5} E_{\mathrm{rot},53}^{21/20} \gamma_{\mathrm{w},4.5}^{1/5} \beta_{\mathrm{b},-1}^{-3/20} t_{\mathrm{sd},0}^{-23/20} \nu_{18}^{-1/10} d_{L28}^{-2}\ \frac{\mathrm{erg}}{\mathrm{cm}^2\ \mathrm{s}}. \tag{63}$$

For sufficiently small values t_{sd} we have $\nu_{\mathrm{bc}}^{\mathrm{SC}} < \nu_{\mathrm{X}} < \nu_{\mathrm{b}m}^{\mathrm{SC}}$ (as t_{sd} increases, then $\nu_{\mathrm{b}m}^{\mathrm{SC}}$ decreases below the X-ray for $t_{\mathrm{sd}} > t_{m,\mathrm{X}}^{\mathrm{SC}}$), and $\nu_{\mathrm{bc}}^{\mathrm{SC}}$ grows above the X-ray for $t_{\mathrm{sd}} > t_{\mathrm{c,X}}^{\mathrm{SC}}$, where the relative ordering of $t_{m,\mathrm{X}}^{\mathrm{SC}}$ and $t_{\mathrm{c,X}}^{\mathrm{SC}}$ depends on the values of the other parameters. For our fiducial values we have

$$t_{m,\mathrm{X}}^{\mathrm{SC}} = 25(1+z)^{-2/3}\eta_{2/3}^{3}\epsilon_{\mathrm{be},1/3}^{8/3}\nu_{bm}^{\mathrm{SC}}\epsilon_{\mathrm{b}B,-3}^{1/3}\xi_{\mathrm{e},1/3}^{-8/3}E_{\mathrm{rot},53}^{1/3}\gamma_{\mathrm{w},4.5}^{8/3}\beta_{\mathrm{b},-1}^{-1}\nu_{18}^{-2/3}\ \mathrm{yr}, \tag{64}$$

$$t_{\mathrm{c,X}}^{\mathrm{SC}} = 80(1+z)^{2/13}a^{4/13}\eta_{2/3}^{7/13}\epsilon_{\mathrm{be},1/3}^{4/13}\epsilon_{\mathrm{b}B,-3}^{3/13}E_{\mathrm{rot},53}^{7/13}\beta_{\mathrm{b},-1}^{-21/13}\nu_{18}^{2/13}\ \mathrm{yr}. \tag{65}$$

For this ordering of these two times we have $\nu_{\mathrm{X}} > \max(\nu_{bm}^{\mathrm{SC}}, \nu_{\mathrm{bc}}^{\mathrm{SC}})$ for $t_{\mathrm{m,X}}^{\mathrm{SC}} < t_{\mathrm{sd}} < t_{\mathrm{c,X}}^{\mathrm{SC}}$, and $\nu_{bm}^{\mathrm{SC}} < \nu_{\mathrm{X}} < \nu_{\mathrm{bc}}^{\mathrm{SC}}$ for $t_{\mathrm{sd}} > t_{\mathrm{c,X}}^{\mathrm{SC}}$. For the other ordering, $t_{\mathrm{c,X}}^{\mathrm{SC}} < t_{\mathrm{m,X}}^{\mathrm{SC}}$, we have $\nu_{\mathrm{X}} < \min(\nu_{bm}^{\mathrm{SC}}, \nu_{\mathrm{bc}}^{\mathrm{SC}})$ for $t_{\mathrm{c,X}}^{\mathrm{SC}} < t_{\mathrm{sd}} < t_{\mathrm{m,X}}^{\mathrm{SC}}$ and $\nu_{bm}^{\mathrm{SC}} < \nu_{\mathrm{X}} < \nu_{\mathrm{bc}}^{\mathrm{SC}}$ for $t_{\mathrm{sd}} > t_{m,\mathrm{X}}^{\mathrm{SC}}$. The X-ray is always below the KN limit, and the SSC $\nu\ F_{\nu}$, is given by

$$\frac{\nu F_{\nu}^{\mathrm{SC}}}{\left(\mathrm{erg\ cm^{-2}\ s^{-1}}\right)} = \begin{cases} 3.7\times10^{-15}(1+z)^{1/2}\eta_{2/3}^{-5/4}\epsilon_{\mathrm{be},1/3}^{-1}\epsilon_{\mathrm{b}B,-3}^{-1/4}\xi_{\mathrm{e},1/3}^{2}E_{\mathrm{rot},53}^{3/4}\gamma_{\mathrm{w},4.5}^{-2}\beta_{\mathrm{b},-1}^{7/4}t_{\mathrm{sd},0}^{-1/4}\nu_{18}^{1/2}d_{L28}^{-2} & t_{\mathrm{sd}} < \min\left(t_{\mathrm{c,X}}^{\mathrm{SC}}, t_{m,\mathrm{X}}^{\mathrm{SC}}\right) \\ 1.8\times10^{-13}(1+z)^{-1/10}\eta_{2/3}^{29/20}\epsilon_{\mathrm{be},1/3}^{7/5}\epsilon_{\mathrm{b}B,-3}^{1/20}\xi_{\mathrm{e},1/3}^{-2/5}E_{\mathrm{rot},53}^{21/20}\gamma_{\mathrm{w},4.5}^{2/5}\beta_{\mathrm{b},-1}^{17/20}t_{\mathrm{sd},0}^{-23/20}\nu_{18}^{-1/10}d_{L28}^{-2} & t_{m,\mathrm{X}}^{\mathrm{SC}} < t_{\mathrm{sd}} < t_3 \\ 2.8\times10^{-14}(1+z)^{-1/10}\eta_{2/3}\epsilon_{\mathrm{be},1/3}^{16/15}\epsilon_{\mathrm{b}B,-3}^{-11/180}\xi_{\mathrm{e},1/3}^{-8/45}E_{\mathrm{rot},53}^{5/6}\gamma_{\mathrm{w},4.5}^{8/45}\beta_{\mathrm{b},-1}^{31/60}t_{\mathrm{sd},0}^{-127/180}\nu_{18}^{-1/10}d_{L28}^{-2} & t_3 < t_{\mathrm{sd}} < t_{\mathrm{c,X}}^{\mathrm{SC}} \\ 2.0\times10^{-5}(1+z)^{4/3}\eta_{2/3}^{5/3}\epsilon_{\mathrm{be},1/3}^{2/3}\epsilon_{\mathrm{b}B,-3}\xi_{\mathrm{e},1/3}^{2}E_{\mathrm{rot},53}^{11/3}\gamma_{\mathrm{w},4.5}^{-2}\beta_{\mathrm{b},-1}^{-7}t_{\mathrm{sd},0}^{-17/3}\nu_{18}^{4/3}d_{L28}^{-2} & t_{\mathrm{c,X}}^{\mathrm{SC}} < t_{\mathrm{sd}} < t_3 \\ 3.0\times10^{-10}(1+z)^{4/3}\eta_{2/3}^{-1}\epsilon_{\mathrm{be},1/3}^{-4/3}\epsilon_{\mathrm{b}B,-3}^{1/3}\xi_{\mathrm{e},1/3}^{10/3}E_{\mathrm{rot},53}^{7/3}\gamma_{\mathrm{w},4.5}^{-10/3}\beta_{\mathrm{b},-1}^{-4}t_{\mathrm{sd},0}^{-3}\nu_{18}^{4/3}d_{L28}^{-2} & t_3 < t_{\mathrm{sd}} < t_{m,\mathrm{X}}^{\mathrm{SC}} \\ 1.2\times10^{-7}(1+z)^{2/5}\eta_{2/3}^{16/5}\epsilon_{\mathrm{be},1/3}^{12/5}\epsilon_{\mathrm{b}B,-3}^{4/5}\xi_{\mathrm{e},1/3}^{-2/5}E_{\mathrm{rot},53}^{14/5}\gamma_{\mathrm{w},4.5}^{2/5}\beta_{\mathrm{b},-1}^{-22/5}t_{\mathrm{sd},0}^{-22/5}\nu_{18}^{2/5}d_{L28}^{-2} & t_{\mathrm{sd}} > \max\left(t_{\mathrm{c,X}}^{\mathrm{SC}}, t_{m,\mathrm{X}}^{\mathrm{SC}}\right). \end{cases} \tag{66}$$

The emission from the PWB calculated above is at the time of the GRB explosion, t_{sd}. However, an important question one needs to address is for how long after the onset of the GRB explosion will the radiation from the plerion persist. Once the SMNS collapses to a black hole, giving rise to the GRB event, the pulsar wind stops abruptly, and no new electrons, freshly accelerated at the wind termination shock, are injected into the plerion from this point onwards. The electrons in the PWB begin to cool radiatively, and adiabatic cooling of the electrons become important on the dynamical time of the plerion, t_{sd} (where this is also a good estimate of the dynamical time for an elongated PWB). Once the final accelerated electrons cool below the Lorentz factor at which they radiate at some observed frequency ν, no more radiation is emitted at that frequency. This cooling time is given by

$$t_{\mathrm{cool}} = 8.9(1+z)^{-1/2}\eta_{2/3}^{-3/4}\epsilon_{\mathrm{be},1/3}^{-1/2}\epsilon_{\mathrm{b}B,-3}^{-1/4}\beta_{\mathrm{b},-1}^{9/4}E_{\mathrm{rot},53}^{-3/4}t_{\mathrm{sd},0}^{9/4}\nu_{9.7}^{-1/2}\ \mathrm{d}, \tag{67}$$

where the above numerical coefficient is for the radio band, while for the optical and X-ray bands the numerical coefficient is 40 min and 24 s, respectively. For our simple example of an elongated PWB, where $\beta_{\mathrm{b}} \approx 1$, the cooling time is approximately two orders of magnitude larger. Owing to the strong dependence on t_{sd}, t_{cool} can become quite large for large values of t_{sd}, especially for radio frequencies.

A possibly more severe constraint arises from the geometrical time delay in the arrival of photons to the observer, from the different parts of the PWB,

$$t_{\mathrm{g}} \sim \frac{R_{\mathrm{b}}}{c} = 24.2\beta_{\mathrm{b},-1}t_{\mathrm{sd},0}\ \mathrm{d}. \tag{68}$$

That is to say, even if the emission from the PWB were to stop at once, with the onset of the GRB, the radiation would still reach the observer t_{g} after the GRB, owing to the geometrical time delay in the arrival of photons to the observer from the far side of the PWB, compared with the side facing the observer. For $t_{\mathrm{sd}} < t_3$, where t_3 is typically rather large (see equation 23), the PWB is in the fast cooling regime, and most of the emission occurs near the radius of the termination shock, R_{s}. This reduces t_{g} by a factor of $R_{\mathrm{s}}/R_{\mathrm{b}}$. However, this is not expected to account for more than a factor of ~5 (KG). For an elongated PWB we have $t_{\mathrm{g}} \sim R_{\mathrm{s}}/c$ for $t_{\mathrm{sd}} \ll t_3$, while for $t_{\mathrm{sd}} > t_3$ we have $t_{\mathrm{g}} \sim R_{\mathrm{p}}/c \approx t_{\mathrm{sd}}$. The emission from the PWB should persist for an observed time of $t_{\mathrm{pl}} \sim (1+z)\max[t_{\mathrm{g}}, \min(t_{\mathrm{sd}}, t_{\mathrm{cool}})]$ after the GRB, which as can be seen from equations (67) and (68) should be at least a few days after the GRB, but can also be much larger ($t_{\mathrm{pl}} \gtrsim t_{\mathrm{g}}$, see equation 68).

The plerion emission at the radio, optical and X-ray bands is shown in Fig. 1. For reference, we also show the times t_{τ} (below which the Thomson optical depth is larger than unity), t_{Fe} (below which iron line features can appear in the X-ray spectrum of the afterglow) and t_{ISM} (for which the effective density of the PWB is similar to that of a typical ISM, i.e. 1 $\mathrm{cm^{-3}}$). In the radio band, the typical limiting flux for detection is ~0.1 mJy, and upper limits at this flux level, at a time $t < t_{\mathrm{pl}}$ after the GRB, would exclude $2 \lesssim t_{\mathrm{sd},0} \lesssim 20$ for $\gamma_{\mathrm{w}} \lesssim 10^5$, while for $2 \lesssim t_{\mathrm{sd},0} \lesssim 65$ this would imply $\gamma_{\mathrm{w}} \gtrsim 10^4$. Values of $t_{\mathrm{sd}} \lesssim 2$ yr or $t_{\mathrm{sd}} \gtrsim 65$ yr are hard to constrain with the radio results.

Optical upper limits at the R band at the level of ~24–25th magnitude ($F_{\nu} \lesssim 0.5$ μJy) would imply $\gamma_{\mathrm{w}} \gtrsim 10^5$ for $t_{\mathrm{sd}} < t_{\mathrm{Fe}}$, i.e. for afterglows with iron lines. More stringent upper limits, may provide more severe constraints. For example, an upper limit of 0.01 μJy [i.e. $R = 28.6$, which might be reached with the *Hubble Space Telescope* (*HST*)] implies $t_{\mathrm{sd}} \gtrsim t_{\mathrm{ISM}}$.

In the X-ray range, for $\gamma_{\mathrm{w}} \lesssim 10^{4.5}$ the SSC emission dominates over the synchrotron emission for all $t_{\mathrm{sd}} \gtrsim t_{\tau}$, and for $\gamma_{\mathrm{w}} = 10^5$ it dominates for $t_{\mathrm{sd}} \gtrsim 7$ yr. The typical limiting flux for detection in the X-ray range is a few$\times10^{-14}$ erg $\mathrm{cm^{-2}\ s^{-1}}$, and upper limits at this level may imply $\gamma_{\mathrm{w}} \gtrsim 10^4$ for $t_{\mathrm{sd}} \lesssim t_{\mathrm{Fe}}$. For $t_{\mathrm{sd}} \gtrsim t_{\mathrm{Fe}}$, such upper limits cannot provide any useful constraints.

5 EFFECTS ON PROMPT GRB EMISSION

Prompt gamma-ray emission is believed to arise from internal shocks within the GRB outflow, owing to variability in its Lorentz factor Γ (Rees & Mészáros 1994; Sari & Piran 1997). In order for this process to be efficient, it needs to occur before the ejecta is significantly

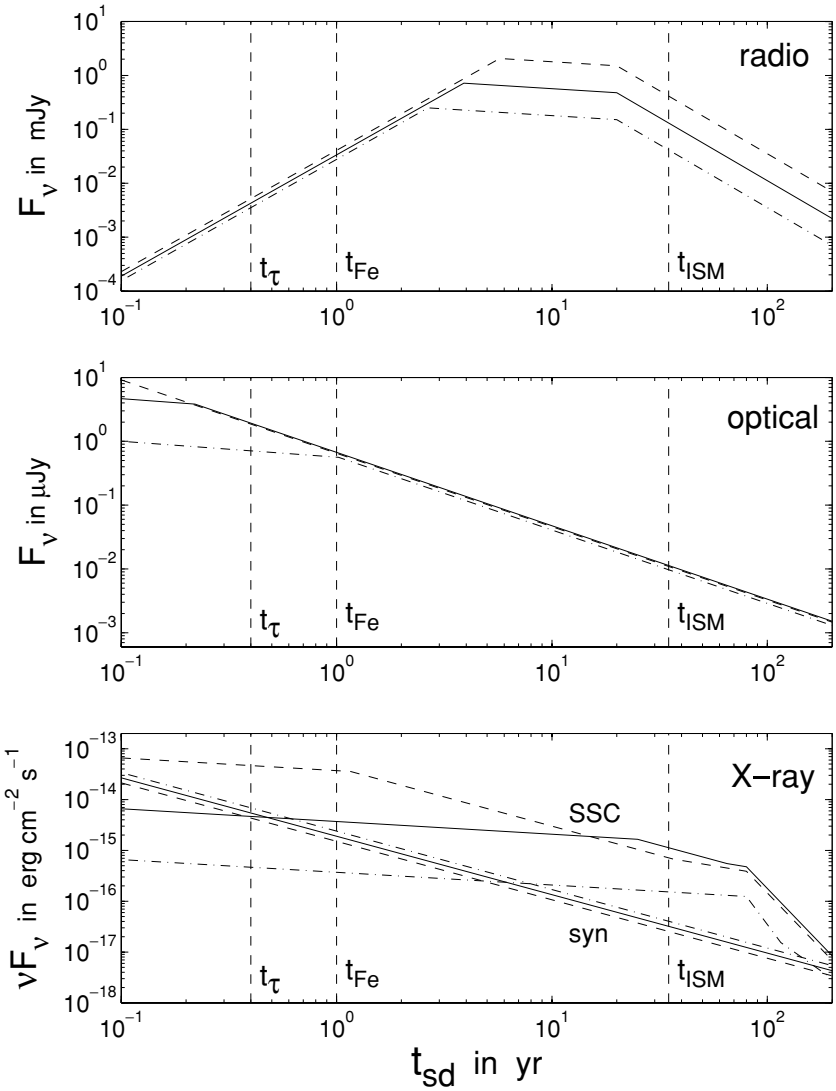

Figure 1. The flux density, F_ν, of the plerion emission at the time of the GRB (i.e. a time t_{sd} after the supernova event), as a function of t_{sd}. The three panels show the flux density in the radio, optical and X-ray bands ($\nu = 5 \times 10^9$, 5×10^{14}, 10^{18} Hz, respectively). For the radio and optical bands we show F_ν of the synchrotron emission, and for the X-ray band we show νF_ν for both the synchrotron and SSC components. The dashed, solid and dot-dashed lines represent $\log10(\gamma_w) = 4$, 4.5 and 5, respectively. Dashed lines are shown at t_τ (below which the Thomson optical depth is larger than unity), t_{Fe} (below which iron line features can appear in the X-ray spectrum of the afterglow) and t_{ISM} (for which the effective density of the PWB is similar to that of a typical ISM, i.e. 1 cm^{-3}.

decelerated by the ambient medium. Therefore, the main effect that a plerionic environment may have on the prompt GRB stage is through inverse Compton scattering of the photons from the external plerion radiation field (which we shall refer to as external Compton, or EC).

The external (plerion) radiation field in the local rest frame of the shocked shells is $U'_{ph,ext} = \Gamma^2 U_{ph,ext}$ where $U_{ph,ext}$ is given by equation (54). The electrons radiatively cool by a combination of synchrotron, SSC and EC processes the time-scales of which are (in the comoving frame) $t'_{syn} \sim 6\pi m_e c/\sigma_T B'^2 \gamma$, $t'_{SC} = t'_{syn}/Y$ and $t'_{EC} = t'_{syn}/X$, where Y is the Compton y-parameter and

$$X = \frac{U'_{ph,ext}}{\epsilon_B e'} = 3.1 \times 10^{-4} a^{1/2} f_{1/3}^{-2} \xi_{e,1/3} \epsilon_{be,1/3}^{-1/2} \epsilon_{bB,-3}^{1/2} \epsilon_e \epsilon_B^{-1} \beta_{b,-1}^{-2} t_{sd,0}^{-3} E_{rot,53} L_{52}^{-1} \Gamma_{2.5}^{8} t_{v,-2}^{2} \tag{69}$$

is the ratio of the energy density of the external radiation field and the magnetic field in the local rest frame of the shocked shells, which is also the ratio between the energies in the EC and synchrotron components. As can be seen from equation (69), $X \ll 1$ for typical parameters. In order to have $X \gtrsim 1$, we need $t_{sd} \lesssim 1$ yr and $\Gamma \gtrsim 10^3$. For an elongated PWB of the type described just before Section 4.1, with $f \sim R_s/R_{eff} \sim 0.1$ and $\beta_b \approx 1$, X is roughly the same.

The EC component is a result of the scattering of external photons from the plerion radiation field by the electrons from the GRB ejecta. This scattering can be done either by hot (relativistic) electrons, or by cold (non-relativistic) electrons, the latter being either in cold shells or cold portions of colliding shells (in either regions before the shock or at a distance larger than $\gamma_c \Delta'$ behind the shock for $\gamma_c < 1$).

For the colliding shells, we assume that the Thomson optical depth, $\tau_{\rm T}$, is smaller than 1. We provide detailed expressions for one representative plerion spectrum, the one given in equation (22), that is relevant for $t_{\rm sd} < t_2 \sim 12$ yr (see equation 35), which is of most interest. Similar expressions for the other plerion spectra can be readily derived in a similar manner. The plerion SSC emission in this regime has a peak for the νF_ν at $\nu_{bm}^{\rm SC} \gtrsim 10^{20}$ Hz for $t_{\rm sd} \lesssim 1$ yr, and will therefore be above the KN cut-off for both hot and cold electrons in the outflowing shells, and its contribution to the EC emission can be neglected. The resulting EC spectrum arising from scattering by the hot electrons is

$$\frac{\nu F_\nu^{EC}}{\nu_m F_{\nu_m}} = X \times \begin{cases} \left(\nu_{\rm sa}^{EC}/\nu_m^{EC}\right)^{1/2}\left(\nu/\nu_{\rm sa}^{EC}\right)^2 & \nu < \nu_{\rm sa}^{EC} \\ \left(\nu/\nu_m^{EC}\right)^{1/2} & \nu_{\rm sa}^{EC} < \nu < \nu_m^{EC} \\ \left(\nu/\nu_m^{EC}\right)^{1-s/2} & \nu_m^{EC} < \nu < \nu_{\rm KN}^{EC}(\gamma_M), \end{cases} \tag{70}$$

where $\nu_{\rm sa}^{EC} \equiv \Gamma^2 \max(\gamma_{\rm c}^2, 1)\nu_{\rm bsa}$ and

$$\nu_m^{EC} = \Gamma^2\gamma_m^2\nu_{bm} \approx 1.9\times 10^{23}\eta_{2/3}^{5/2}\epsilon_{{\rm be},1/3}^2\epsilon_{{\rm b}B,-3}^{1/2}\xi_{{\rm e},1/3}^{-2}E_{{\rm rot},53}^{1/2}\gamma_{{\rm w},4.5}^2\beta_{{\rm b},-1}^{-3/2}t_{{\rm sd},0}^{-3/2}\epsilon_{\rm e}^2\Gamma_{2.5}^2 \text{ Hz},$$

$$\nu_{{\rm KN},1}^{\rm SC} = \frac{\nu_{{\rm KN},0}^2}{\nu_{bm}} \approx 3.0\times 10^{27}\eta_{2/3}^{-5/2}\epsilon_{{\rm be},1/3}^{-2}\epsilon_{{\rm b}B,-3}^{-1/2}\xi_{{\rm e},1/3}^2E_{{\rm rot},53}^{-1/2}\gamma_{{\rm w},4.5}^{-2}\beta_{{\rm b},-1}^{-3/2}t_{{\rm sd},0}^{3/2} \text{ Hz},$$

$$\nu_{\rm KN}^{\rm SC}(\gamma_M) = \Gamma\gamma_M\nu_{{\rm KN},0} \approx 6.6\times 10^{27}(1+Y+X)^{-1/2}\epsilon_{\rm e}^{1/4}\epsilon_B^{-1/4}L_{52}^{-1/4}\Gamma_{2.5}^{5/2}t_{\nu,-2}^{1/2} \text{ Hz}. \tag{71}$$

If $\nu_{{\rm KN},1}^{\rm SC} < \nu_{\rm KN}^{\rm SC}(\gamma_M)$ then we have $\nu F_\nu \propto \nu^{1/2-s}$ for $\nu_{{\rm KN},1}^{\rm SC} < \nu < \nu_{\rm KN}^{\rm SC}(\gamma_M)$. The peak of the νF_ν^{EC} spectrum, of the EC component from hot electrons is $\sim 10^{-10}(X/10^{-4})$ erg cm^{-2} s^{-1} and is a factor of $X \sim 10^{-4}$ (for $t_{\rm sd} \sim 1$ yr) smaller than that of the synchrotron component and therefore might be detected only for extreme parameters ($t_{{\rm sd},0} \lesssim 1$, $\Gamma \gtrsim 10^3$).

For the scattering by cold electrons, the optical depth is approximately

$$\tau_{\rm T} = \sigma_t n_{\rm e}'\Delta' \approx 0.02\epsilon_{\rm e}^{-1}L_{52}\Gamma_{2.5}^{-5}t_{\nu,-2}^{-1}, \tag{72}$$

and the Compton y-parameter is $Y = \min(\tau_{\rm T}, 1)\Gamma^2$. This implies that all frequencies of the plerion spectrum are shifted upwards by a factor of Γ^2, and the corresponding flux density, F_ν, should be multiplied by $\min(\tau_{\rm T}, 1)$. The only exception to this simple re-scaling is that the spectral slope below the upscattered self-absorption frequency will be $F_\nu \propto \nu$, instead of ν^2 in the plerion spectrum. The peak of the νF_ν^{EC} spectrum will be at

$$\Gamma^2\nu_{bm} \approx 5.1\times 10^{18}(1+z)^{-1}\eta_{2/3}^{5/2}\epsilon_{{\rm be},1/3}^2\epsilon_{{\rm b}B,-3}^{1/2}\xi_{{\rm e},1/3}^{-2}E_{{\rm rot},53}^{1/2}\gamma_{{\rm w},4.5}^2\beta_{{\rm b},-1}^{-3/2}t_{{\rm sd},0}^{-3/2} \text{ Hz}, \tag{73}$$

which is typically in the hard X-ray or soft gamma-ray range for $t_{\rm sd} \lesssim 1$ yr. However, the peak of νF_ν^{EC} for this component is a factor of $Y \leqslant \Gamma^2 \sim 10^5$ larger than $\nu_{bm}F_{\nu_{bm}} \lesssim 10^{-14}$ erg cm^{-2} s^{-1} and is therefore $\lesssim 10^{-9}$ erg cm^{-2}s^{-1}, and will typically hide below the standard GRB emission.

Another possible effect of the plerion radiation field is that photons with energy $\gtrsim 1\, t_{{\rm sd},0}^2$ GeV cannot escape the emission region owing to a large opacity to pair production ($\tau_{\gamma\gamma} > 1$). Therefore, all the components of the prompt GRB emission, including synchrotron, SSC and EC, will have an upper cut-off at this photon energy.

Finally, we consider the effect of the Compton drag caused by the plerion radiation field on the GRB outflow.[6] The effect of Compton drag in GRBs was considered in the context of the collapsar model, where the radiation comes from the walls of a funnel along the rotational axis of the progenitor star (Ghisellini et al. 2000; Lazzati et al. 2000). The rate of energy loss of a shell of initial Lorentz factor Γ_0 rest mass M and solid angle Ω_j, is given by

$$\frac{{\rm d}E}{{\rm d}t} = \frac{{\rm d}\Gamma}{{\rm d}t}Mc^2 = -\Omega_j R^2 c\Gamma^2 U_{\rm ph}\min(\tau_{\rm T}, 1), \tag{74}$$

where $t \approx R/c$ is the laboratory frame time, $\tau_{\rm T} = (R/R_\tau)^{-2}$ is the Thomson optical depth of the shell, R_τ is the radius where this optical depth drops below unity.[7] We render equation (74) dimensionless by introducing $\tilde{R} \equiv R/R_\tau = \tau_{\rm T}^{-1/2}$,

$$\frac{d(1/\Gamma)}{d\tilde{R}} = A\min(\tilde{R}^2, 1), \quad A \equiv \frac{\Omega_j U_{\rm ph}R_\tau^3}{Mc^2}. \tag{75}$$

This gives

$$\frac{\Gamma(\tilde{R})}{\Gamma_0} = \begin{cases} (1+A\Gamma_0\tilde{R}^3/3)^{-1} & \tilde{R} < 1 \\ \left[1+A\Gamma_0(\tilde{R}-2/3)\right]^{-1} & \tilde{R} > 1, \end{cases} \tag{76}$$

where

$$R_\tau = 3.3\times 10^{12}\epsilon_\gamma^{-1/2}L_{52}^{1/2}\Gamma_{2.5}^{-1/2}t_{\nu,-2}^{1/2} \text{ cm},$$

$$A = 1.6\times 10^{-8}af_{1/3}^{-2}\epsilon_\gamma^{-1/2}\xi_{{\rm e},1/3}E_{{\rm rot},53}\beta_{{\rm b},-1}^{-2}t_{{\rm sd},0}^{-3}L_{52}^{1/2}\Gamma_{2.5}^{-1/2}t_{\nu,-2}^{1/2}, \tag{77}$$

[6] The emission from the initial supernova itself always contributes much less to the total radiation field inside the PWB, and may therefore be neglected.

[7] We have used the total photon energy density of the PWB, $U_{\rm ph}$, which includes the SSC component, even though for $t_{\rm sd} \lesssim 30$ yr, most of the energy in the SSC component is in photons that are above the Klein–Nishina limit, and would therefore have a reduced cross-section for scattering. Since we show that Compton drag is unimportant even without taking into account the reduced cross-section, this effect can only strengthen our conclusion.

where ϵ_γ is the fraction of the kinetic luminosity of the GRB outflow that is converted into gamma-ray emission. As can be seen from equations (76) and (77), $A\Gamma_0 \ll 1$ and therefore $\Gamma(R_\tau) \cong \Gamma_0$, while for $R \gg R_\tau$ the fractional change in Γ is given by $A\Gamma_0\tilde{R}$. If the radius, $R_{\rm cd}$, at which deceleration caused by Compton drag becomes significant, is larger than the deceleration radius, $R_{\rm dec} \approx f R_{\rm b}$, owing to the sweeping up of the PWB material, then the deceleration caused by Compton drag is at most comparable to (and never dominant over) the deceleration caused by the ambient medium, for[8] $k \leqslant 1$. Therefore, Compton drag will have a significant effect on the deceleration only if $R_{\rm cd} < R_{\rm dec}$, which for our fiducial values may be expressed as $t_{\rm sd} < 0.3\ f^{1/2}$yr. For such low values of $t_{\rm sd}$ the SNR shell is still optically thick to Compton scattering ($t_{\rm sd} < t_\tau$), so that we do not expect to see the GRB or afterglow emission. We conclude that the deceleration of the GRB ejecta caused by Compton drag is negligible for relevant values of $t_{\rm sd}$.

6 EFFECTS ON THE AFTERGLOW EMISSION

At a time $t_{\rm sd}$ after the supernova event, the SMNS collapses and triggers the GRB explosion, sending a fireball and relativistic blast wave into the PWB. When the GRB ejecta has swept up enough of the outlying material, it is decelerated, and it drives a strong relativistic shock into the external medium, that is responsible for the afterglow emission.

In this section we study the observational consequences of the plerionic environment inside the PWB that are different from the standard 'cold', weakly magnetized proton–electron external medium. One of the advantages of having the PWB as the environment for the GRB afterglow is that it naturally yields high values of $\epsilon_{\rm e}$ and ϵ_B (the fraction of the internal energy in the electrons and in the magnetic field, respectively) behind the AG shock (KG). High values of $\epsilon_{\rm e}$ are expected from the fact that relativistic pulsar-type winds are probably dominated by an electron–positron component, whereas significant values of ϵ_B should naturally occur if the winds are characterized by a high magnetization parameter. We expect $\epsilon_B \sim \epsilon_{{\rm b}B}$, and use the same fiducial value for these two parameters. The electrons in the PWB are typically colder than the protons by the time the afterglow shock arrives, and most of the energy is in the internal energy of the hot protons. This might suggest that $\epsilon_{\rm e}$ can be slightly smaller than $\epsilon_{\rm be}$ and motivates us to use $\epsilon_{\rm e} = \epsilon_{{\rm e},-1}/10$ for our fiducial values.

The values of the physical quantities behind the AG shock can be determined from the appropriate generalizations of the hydrodynamic conditions used in the case of a 'cold' medium, taking into account the fact that the pre-shock gas is now 'hot' and should be well described by a relativistic equation of state, $p = e/3 = w/4$, where w is the enthalpy density and p is the particle pressure. In the following we largely follow the analysis of KG. The deceleration of the AG shock is determined by the total enthalpy of the external medium, $w_{\rm tot}$, which includes contributions from the particles and the magnetic field enthalpy, $B^2/4\pi$, where the latter contribution is negligible for our choice of parameters ($\epsilon_B \ll 1$). This make it convenient to define an 'equivalent' hydrogen number density $n_{\rm H,equiv} \equiv w_{\rm tot}/m_{\rm p}c^2 \approx w/m_{\rm p}c^2 = (4/3)\ e/m_{\rm p}c^2$, in analogy with the traditional parametrization of the external medium enthalpy density, $w = n_{\rm H}\ m_{\rm p}\ c^2$, which is relevant for a standard ISM or stellar-wind environment.

In general, both the energy and the electron number density may be a function of the distance r from the centre of the PWB and can be parametrized as

$$e(r) = A_{\rm e} r^{-k_*}, \qquad A_{\rm e} = \frac{(3-k_*)\eta E_{\rm rot}}{4\pi R_{\rm b}^{3-k}}, \tag{78}$$

$$n_{\rm e}(r) = A_n r^{-k}, \qquad A_n = \frac{(3-k)N_{\rm e}}{4\pi R_{\rm b}^{3-k}}, \tag{79}$$

where $N_{\rm e} = \dot{N}_{\rm e} t_{\rm sd}$ is the total number of electrons in the PWB and $\dot{N}_{\rm e}$ is given in equation (10). When a large fraction of the energy density in the PWB goes to the proton component we have $\eta \sim 1$ and we can expect both $n_{\rm H,equiv}$ and $n_{\rm e}$ to have a similar radial dependence, i.e. $k = k_*$. The expected values of k typically range between $k = 0$, similar to the ISM, and $k = 1$, which is intermediate between an ISM and a stellar wind (KG). For an elongated PWB, things can become much more complicated, since e and $n_{\rm e}$ can depend not only on r but also on the angle θ from the polar axis. However, if the θ dependence within the opening angle of the GRB jet is small, and the dependence on r may be reasonably approximated by a power law, then our formalism still holds for $k \approx 0$, with the usual substitution of $\beta_{\rm b} = 3R_{\rm eff}/2ct_{\rm sd}$ (see the beginning of Section 4). For $k > 0$ we also need to change the normalization in equations (78) and (79) accordingly.

The expressions for the radius $R_{\rm AG}$ and the Lorentz factor $\Gamma_{\rm AG}$ of the shocked AG material can be derived using energy conservation,

$$E_{\rm iso} = \Gamma_{\rm AG}^2 \int_{R_S}^{R_{\rm AG}} n_{\rm H,equiv} m_{\rm p} c^2 4\pi r^2\ {\rm d}r, \tag{80}$$

where $E_{\rm iso}$ is the isotropic equivalent energy of the AG shock, and using the relation

$$t \sim \frac{R_{\rm AG}}{4c\Gamma_{\rm AG}^2}, \tag{81}$$

where t is the observed time. We obtain

$$R_{\rm AG} = \left(\frac{3E_{\rm iso} ct R_{\rm b}^{3-k}}{\eta E_{\rm rot}}\right)^{1/(4-k)} \tag{82}$$

[8] This is since the Lorentz factor decreases with radius as R^{-1} caused by Compton drag and as $R^{(k-3)/2}$ caused by the ambient medium.

$$\Gamma_{\rm AG} = \sqrt{\frac{R_{\rm AG}}{4ct}} \propto t^{(k-3)/2(4-k)} \propto \begin{cases} t^{-3/8} & k=0 \\ t^{-1/3} & k=1. \end{cases} \tag{83}$$

The post-shock energy and particle density (in the shock comoving frame) are given by

$$e' = 4\Gamma_{\rm AG}^2 w, \quad n'_{\rm e} = 4\Gamma_{\rm AG} n_{\rm e}. \tag{84}$$

The electron distribution is assumed to be similar to that of internal shocks, $N(\gamma) \propto \gamma^{-p}$ for $\gamma_m < \gamma < \gamma_M$, and we use $p = 2.5$ to obtain the numerical values.

As mentioned in Section 4.4, the plerion radiation field is roughly homogeneous and isotropic within the radius $fR_{\rm b}$ where the plerion emission takes place. At $r \lesssim fR_{\rm b}$ the external (plerion) photon energy density, $U_{\rm ph,ext}$, is given by equation (54), and we may use the relation $U'_{\rm ph,ext} = \Gamma_{\rm AG}^2 U_{\rm ph,ext}$ (which is valid for an isotropic radiation field) to obtain

$$X = \frac{U'_{\rm ph,ext}}{\epsilon_B e'} \approx \begin{cases} 2.1 a^{1/2} f_{1/3}^{-2} \eta_{2/3}^{-1} \epsilon_{{\rm be},1/3}^{-1/2} \epsilon_{{\rm b}B,-3}^{1/2} \epsilon_{B,-3}^{-1} \xi_{{\rm e},1/3} \beta_{{\rm b},-1} & k=0 \\ 1.8 a^{1/2} f_{1/3}^{-2} \eta_{2/3}^{-4/3} \epsilon_{{\rm be},1/3}^{-1/2} \epsilon_{{\rm b}B,-3}^{1/2} \epsilon_{B,-3}^{-1} \xi_{{\rm e},1/3} E_{{\rm rot},53}^{-1/3} \beta_{{\rm b},-1}^{2/3} t_{{\rm sd},1.5}^{-1/3} E_{{\rm iso},53}^{1/3} t_{\rm d}^{1/3} & k=1, \end{cases} \tag{85}$$

where $t_{{\rm sd},1.5} = t_{\rm sd}/10^{3/2}$. For $t_{\rm sd} > t_3 \sim 65$ yr the PWB is slow cooling, and $f = 1$, so that $R_{\rm AG} < fR_{\rm b}$ throughout the afterglow. For $t_{\rm sd} < t_3$ the plerion emission is radiated within a shell of width $R_{\rm b} - R_{\rm s}$ times the ratio, $(t_{\rm sd}/t_3)^2$, of the cooling time of electrons with $\gamma_{{\rm b}m}$, and the dynamical time $t_{\rm sd}$. This implies that generally, $f = \min\{1, (R_{\rm s}/R_{\rm b})[1 - (t_{\rm sd}/t_3)^2] + (t_{\rm sd}/t_3)^2\}$. For $t_{\rm sd} < t_3$ we have $f < 1$ and therefore $R_{\rm AG} < fR_{\rm b}$ only at sufficiently early times after the GRB. For $t_{\rm sd} \ll t_3$, the radiation is emitted within a thin shell behind the wind termination shock, at $R_{\rm s}$, and $f \approx R_{\rm s}/R_{\rm b}$. In this case $R_{\rm AG} > fR_{\rm b}$ throughout the afterglow. We study the implications in the following.

At $r > fR_{\rm b}$, the plerion radiation field is no longer isotropic or homogeneous, and we model the plerion radiation field as resulting from emission by a uniformly bright sphere with a radius $fR_{\rm b}$, and obtain

$$U_{\rm ph} = \frac{\xi_{\rm e} L_{\rm w}}{2\pi c f R_{\rm b}^2}(1-\mu) \approx \frac{\xi_{\rm e} L_{\rm w}}{4\pi c r^2}, \qquad U'_{\rm ph} = \frac{\xi_{\rm e} L_{\rm w}}{2\pi c f R_{\rm b}^2} \frac{\Gamma_{\rm AG}^2}{3\beta}[(1-\beta\mu)^3 - (1-\beta)^3], \tag{86}$$

where $\mu \equiv [1 - (fR_{\rm b}/r)^2]^{1/2}$ and $\beta = (1 - \Gamma_{\rm AG}^{-2})^{1/2}$. The ratio of the photon energy in the local and the observer frames is now

$$\frac{U'_{\rm ph}}{U_{\rm ph}} = \frac{\Gamma_{\rm AG}^2 \left[(1-\beta\mu)^3 - (1-\beta)^3\right]}{3\beta(1-\mu)} \approx \begin{cases} \Gamma_{\rm AG}^2 (1-\mu)^2/3 \approx (fR_{\rm b}/r)^4 \Gamma_{\rm AG}^2/12 & r \ll \Gamma_{\rm AG} fR_{\rm b} \\ (1-\beta)/(1+\beta) \approx 1/4\Gamma_{\rm AG}^2 & r \gg \Gamma_{\rm AG} fR_{\rm b}. \end{cases} \tag{87}$$

During the early afterglow, $R_{\rm AG}$ is relatively small and $\Gamma_{\rm AG} \gg 1$, so that $R_{\rm AG} \ll \Gamma_{\rm AG}\, fR_{\rm b}$, and the first limit of equation (87) is applicable, implying

$$X_1 \approx \begin{cases} 0.26 a^{-1/2} f_{1/3}^4 \eta_{2/3}^{1/2} \epsilon_{{\rm be},1/3}^{-1/2} \epsilon_{{\rm b}B,-3}^{1/2} \epsilon_{B,-3}^{-1} \xi_{{\rm e},1/3} E_{{\rm rot},53}^{3/2} \beta_{{\rm b},-1}^{5/2} t_{{\rm sd},1.5}^{3/2} E_{{\rm iso},53}^{-3/2} t_{\rm d}^{-3/2} & k=0 \\ 0.93 a^{-1/2} f_{1/3}^4 \eta_{2/3}^{2/3} \epsilon_{{\rm be},1/3}^{-1/2} \epsilon_{{\rm b}B,-3}^{1/2} \epsilon_{B,-3}^{-1} \xi_{{\rm e},1/3} E_{{\rm rot},53}^{5/3} \beta_{{\rm b},-1}^{8/3} t_{{\rm sd},1.5}^{5/3} E_{{\rm iso},53}^{-5/3} t_{\rm d}^{-5/3} & k=1. \end{cases} \tag{88}$$

During the course of the afterglow its radius increases while its Lorentz factor decreases, so that eventually $R_{\rm AG}$ becomes larger than $\Gamma_{\rm AG}\, fR_{\rm b}$, and the second limit of equation (87) becomes relevant, implying

$$X_2 \approx \begin{cases} 1.3 \times 10^{-4} a^{-1/2} \epsilon_{{\rm be},1/3}^{-1/2} \epsilon_{{\rm b}B,-3}^{1/2} \epsilon_{B,-3}^{-1} \xi_{{\rm e},1/3} E_{{\rm rot},53} t_{{\rm sd},1.5}^{3/2} E_{{\rm iso},53}^{-1} t_{\rm d} & k=0 \\ 2.0 \times 10^{-4} a^{-1/2} \epsilon_{{\rm be},1/3}^{-1/2} \epsilon_{{\rm b}B,-3}^{1/2} \epsilon_{B,-3}^{-1} \xi_{{\rm e},1/3} E_{{\rm rot},53} t_{{\rm sd},1.5}^{3/2} E_{{\rm iso},53}^{-1} t_{\rm d} & k=1, \end{cases} \tag{89}$$

as long as the afterglow shock is still relativistic. One can combine the two limits and use $X = \max(X_1, X_2)$. However, since the region where these asymptotic expressions for X are not a very good approximation may play an important role, we use equation (86) rather than equations (88) and (89) for all our calculations.

It is also worth noting that the average shift in frequency of the photons between the observer frame and the local and the rest frame is $\langle \nu'/\nu \rangle = \Gamma_{\rm AG}[1 - \beta(1+\mu)/2] \approx [1 + \Gamma_{\rm AG}^2(1-\mu)^2]/2\Gamma_{\rm AG}$, and varies between $\Gamma_{\rm AG}/2$ and $1/2\Gamma_{\rm AG}$. This should be compared with the usual factor of $\Gamma_{\rm AG}$ for an isotropic (plerion) radiation field, and implies lower typical EC frequencies, by a factor of $[1 - \beta(1+\mu)/2]$. For simplicity we do not include this factor in the expressions for the EC frequencies, but we do take it into account in Fig. 2, and when deriving constraints on the model parameters.

The electron cooling time is $t_{\rm syn}/(1 + Y + X)$ where the Compton y-parameter may be obtained by solving the equation

$$Y \approx \tau_{\rm T} a \gamma_{\rm c} \gamma_m \approx \frac{a\epsilon_{\rm e}}{\epsilon_B(1 + Y + X)}, \tag{90}$$

which gives (Granot & Königl 2001)

$$Y \approx \begin{cases} \sqrt{a\epsilon_{\rm e}/\epsilon_B} & 1, X^2 \ll a\epsilon_{\rm e}/\epsilon_B \\ a\epsilon_{\rm e}/\epsilon_B & X, a\epsilon_{\rm e}/\epsilon_B \ll 1 \\ a\epsilon_{\rm e}/(\epsilon_B X) & a\epsilon_{\rm e}/\epsilon_B, 1 \ll X^2. \end{cases} \tag{91}$$

For our choice of parameters, $\epsilon_B \ll \epsilon_{\rm e}$ and $a\epsilon_{\rm e}/\epsilon_B \gg 1$, so that either the first or the third limits of equation (91) are relevant. As the first limit is more often applicable, we use the parametrization $(1 + Y + X) \equiv \bar{X}(a\epsilon_{\rm e}/\epsilon_B)^{1/2}$, so that the numerical coefficients and explicit dependence on the parameters of the break frequencies (that depend on the electron cooling time), would be relevant for $X^2 \ll a\epsilon_{\rm e}/\epsilon_B$, where $\bar{X} \approx 1$. In the limit $X^2 \gg a\epsilon_{\rm e}/\epsilon_B$, the numerical coefficients and parameter dependences change because of the dependence on $\bar{X} \approx X/(a\epsilon_{\rm e}/\epsilon_B)^{1/2}$, which is no longer close to 1 in this limit.

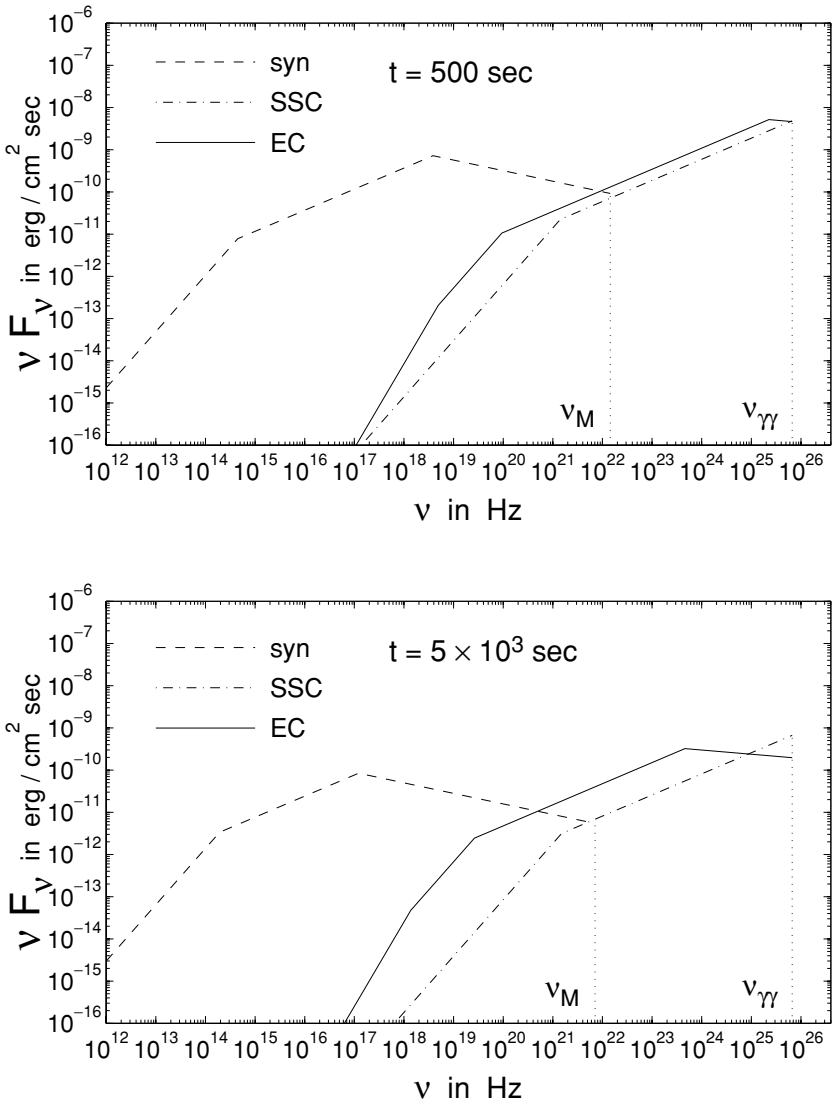

Figure 2. The afterglow νF_ν spectrum at $t = 500$ s (upper panel) and 5×10^3 s (lower panel) after the GRB, for our fiducial parameters, and for $t_{\rm sd} = 20$ yr, $E_{\rm rot,53} = 0.5$, $z = 1$, $R_{\rm s}/R_{\rm b} = 0.1$. Dotted vertical lines indicate ν_M where the upper cut-off for the synchrotron emission is located, and $\nu_{\gamma\gamma}$ where the upper cut-off of the SSC and EC (owing to pair opacity) is located.

6.1 The synchrotron emission

In the standard case of a uniform ambient medium, one can express the break frequencies and the peak flux in terms of the shock energy E, the ambient density $n_{\rm H}$, the observed time t and $\epsilon_{\rm e}$, ϵ_B, and the distance to the source (Sari, Piran & Narayan 1998). This is thanks to the fact that for a 'standard' external medium that is composed of equal numbers of protons and electrons, so that both the shock dynamics (that is determined by $w = n_{\rm H} m_{\rm p} c^2$) and the external number density of electrons (that enter the expressions for the flux normalization and self-absorption frequency), are determined by a single parameter, $n_{\rm H}$. In the case of a shock propagating inside a PWB, the dynamics of the AG shock are determined by $w = n_{\rm H,equiv}\, m_{\rm p} c^2 \approx \eta \gamma_{\rm w} n_{\rm p} m_{\rm p} c^2$, i.e. dominated by the internal energy of the hot protons, while the number density of electrons is different, and is dominated by the electron–positron pairs. We find

$$n_{\rm H,equiv} = \frac{\eta E_{\rm rot}}{\pi R_{\rm b}^3 m_{\rm p} c^2} \approx 1.8 \eta_{2/3} E_{\rm rot,53} \beta_{\rm b,-1}^{-3} t_{\rm sd,1.5}^{-3},$$

$$\frac{n_{\rm e}}{n_{\rm H,equiv}} = \frac{3\xi_{\rm e} m_{\rm p}}{4\eta_{\rm e}\gamma_{\rm w} m_{\rm e}} \approx 0.022 \eta_{2/3}^{-1} \xi_{\rm e,1/3} \gamma_{\rm w,4.5}^{-1}. \tag{92}$$

For an elongated PWB we can make the usual substitution $\beta_{\rm b} = 3R_{\rm eff}/2ct_{\rm sd}$, to obtain the relevant expressions (see the discussion just before Section 4.1).

The self-absorption frequency is typically $\nu_{\rm sa} < \min(\nu_{\rm c}, \nu_m)$, and is calculated using equation (30) for fast cooling and equation (34) for slow cooling, solving for $\tau'_\nu = \alpha' R_{\rm AG}/\Gamma_{\rm AG} = 1$ for $\nu'_{\rm sa}$ and then $\nu_{\rm sa} = \Gamma_{\rm AG}\nu'_{\rm sa}$. The transition time from fast to slow cooling, t_0, is obtained by equating $\gamma_{\rm c}$ and γ_m. For $k = 0$ we obtain

$$\begin{aligned}
&\nu_{\rm c} \approx 2.1\times 10^{14}(1+z)^{-1/2}a^{-1}\bar{X}^{-2}\eta_{2/3}^{-1}\epsilon_{{\rm e},-1}^{-1}\epsilon_{B,-3}^{-1/2}E_{{\rm rot},53}^{-1}\beta_{{\rm b},-1}^{3}t_{{\rm sd},1.5}^{3}E_{{\rm iso},53}^{-1/2}t_{\rm d}^{-1/2}\ {\rm Hz},\\
&\nu_m \approx 1.2\times 10^{15}(1+z)^{1/2}\eta_{2/3}^{2}\xi_{{\rm e},1/3}^{-2}\epsilon_{{\rm e},-1}^{2}\epsilon_{B,-3}^{1/2}\gamma_{{\rm w},4.5}^{2}E_{{\rm iso},53}^{1/2}t_{\rm d}^{-3/2}\ {\rm Hz},\\
&\nu_M \approx 5.2\times 10^{21}(1+z)^{-5/8}a^{-1/2}\bar{X}^{-1}\eta_{2/3}^{-1/8}\epsilon_{{\rm e},-1}^{-1/2}\epsilon_{B,-3}^{1/2}E_{{\rm rot},53}^{-1/8}\beta_{{\rm b},-1}^{3/8}t_{{\rm sd},1.5}^{3/8}E_{{\rm iso},53}^{1/8}t_{\rm d}^{-3/8}\ {\rm Hz},\\
&\nu_{\rm sa1} \approx 1.0\times 10^{8}(1+z)^{-1/2}\bar{X}\eta_{2/3}^{1/2}\xi_{{\rm e},1/3}^{3/5}\epsilon_{{\rm e},-1}^{1/2}\epsilon_{B,-3}^{7/10}E_{{\rm rot},53}^{11/10}\gamma_{{\rm w},4.5}^{-3/5}\beta_{{\rm b},-1}^{-3.3}t_{{\rm sd},1.5}^{-3.3}E_{{\rm iso},53}^{7/10}t_{\rm d}^{-1/2}\ {\rm Hz},\\
&\nu_{\rm sa2} \approx 2.6\times 10^{7}(1+z)^{-1}\eta_{2/3}^{-1}\xi_{{\rm e},1/3}^{8/5}\epsilon_{{\rm e},-1}^{-1}\epsilon_{B,-3}^{1/5}E_{{\rm rot},53}^{3/5}\gamma_{{\rm w},4.5}^{-8/5}\beta_{{\rm b},-1}^{-9/5}t_{{\rm sd},1.5}^{-9/5}E_{{\rm iso},53}^{1/5}\ {\rm Hz},\\
&F_{\nu,\max} \approx 0.61(1+z)\eta_{2/3}^{-1/2}\xi_{{\rm e},1/3}\epsilon_{B,-3}^{1/2}E_{{\rm rot},53}^{1/2}\gamma_{{\rm w},4.5}^{-1}\beta_{{\rm b},-1}^{-3/2}t_{{\rm sd},1.5}^{-3/2}E_{{\rm iso},53}d_{L28}^{-2}\ {\rm mJy},\\
&t_0 \approx 5.7(1+z)\bar{X}^{2}\eta_{2/3}^{3}\xi_{{\rm e},1/3}^{-2}\epsilon_{{\rm e},-1}^{3}\epsilon_{B,-3}E_{{\rm rot},53}\gamma_{{\rm w},4.5}^{2}\beta_{{\rm b},-1}^{-3}t_{{\rm sd},1.5}^{-3}E_{{\rm iso},53}\ {\rm d},
\end{aligned} \tag{93}$$

where $\nu_{\rm sa1}$ is for fast cooling and $\nu_{\rm sa2}$ is for slow cooling. For $k=1$ we obtain

$$\begin{aligned}
&\nu_{\rm c} \approx 7.0\times 10^{13}(1+z)^{-5/6}a^{-1}\bar{X}^{-2}\eta_{2/3}^{-4/3}\epsilon_{{\rm e},-1}^{-1}\epsilon_{B,-3}^{-1/2}E_{{\rm rot},53}^{-4/3}\beta_{{\rm b},-1}^{8/3}t_{{\rm sd},1.5}^{8/3}E_{{\rm iso},53}^{-1/6}t_{\rm d}^{-1/6}\ {\rm Hz},\\
&\nu_m \approx 9.9\times 10^{14}(1+z)^{1/2}\eta_{2/3}^{2}\xi_{{\rm e},1/3}^{-2}\epsilon_{{\rm e},-1}^{2}\epsilon_{B,-3}^{1/2}\gamma_{{\rm w},4.5}^{2}E_{{\rm iso},53}^{1/2}t_{\rm d}^{-3/2}\ {\rm Hz},\\
&\nu_M \approx 4.2\times 10^{21}(1+z)^{-2/3}a^{-1/2}\bar{X}^{-1}\eta_{2/3}^{-1/6}\epsilon_{{\rm e},-1}^{-1/2}\epsilon_{B,-3}^{1/2}E_{{\rm rot},53}^{-1/6}\beta_{{\rm b},-1}^{1/3}t_{{\rm sd},1.5}^{1/3}E_{{\rm iso},53}^{1/6}t_{\rm d}^{-1/3}\ {\rm Hz},\\
&\nu_{\rm sa1} \approx 3.3\times 10^{8}(1+z)^{-2/15}\bar{X}\eta_{2/3}^{13/15}\xi_{{\rm e},1/3}^{3/5}\epsilon_{{\rm e},-1}^{1/2}\epsilon_{B,-3}^{7/10}E_{{\rm rot},53}^{22/15}\gamma_{{\rm w},4.5}^{-3/5}\beta_{{\rm b},-1}^{-44/15}t_{{\rm sd},1.5}^{-44/15}E_{{\rm iso},53}^{1/3}t_{\rm d}^{-13/15}\ {\rm Hz},\\
&\nu_{\rm sa2} \approx 5.2\times 10^{7}(1+z)^{-4/5}\eta_{2/3}^{-4/5}\xi_{{\rm e},1/3}^{8/5}\epsilon_{{\rm e},-1}^{-1}\epsilon_{B,-3}^{1/5}E_{{\rm rot},53}^{4/5}\gamma_{{\rm w},4.5}^{-8/5}\beta_{{\rm b},-1}^{-8/5}t_{{\rm sd},1.5}^{-8/5}t_{\rm d}^{-1/5}\ {\rm Hz},\\
&F_{\nu,\max} \approx 1.2(1+z)^{7/6}\eta_{2/3}^{-1/3}\xi_{{\rm e},1/3}\epsilon_{B,-3}^{1/2}E_{{\rm rot},53}^{2/3}\gamma_{{\rm w},4.5}^{-1}\beta_{{\rm b},-1}^{-4/3}t_{{\rm sd},1.5}^{-4/3}E_{{\rm iso},53}^{5/6}t_{\rm d}^{-1/6}d_{L28}^{-2}\ {\rm mJy},\\
&t_0 \approx 7.3(1+z)\bar{X}^{3/2}\eta_{2/3}^{5/2}\xi_{{\rm e},1/3}^{-3/2}\epsilon_{{\rm e},-1}^{9/4}\epsilon_{B,-3}^{3/4}E_{{\rm rot},53}\gamma_{{\rm w},4.5}^{3/2}\beta_{{\rm b},-1}^{-2}t_{{\rm sd},1.5}^{-2}E_{{\rm iso},53}^{1/2}\ {\rm d}.
\end{aligned} \tag{94}$$

We note that in order for $\nu_{\rm sa}$ not to exceed a few GHz, as typically implied by observations, we need $t_{\rm sd} \gtrsim 10$ yr. This also gives more reasonable values for the transition time from fast to slow cooling, t_0, and for $F_{\nu,\max}$. For $k=0$ the effective mass density of the PWB becomes similar to that of a typical ISM, $n_{\rm H,equiv} = 1\ {\rm cm}^{-3}$, for

$$t_{\rm ISM} = 38\eta_{2/3}^{1/3}E_{{\rm rot},53}^{1/3}\beta_{{\rm b},-1}^{-1}\ {\rm yr}, \tag{95}$$

while the electron number density reaches the same value for a smaller $t_{\rm sd} = 10.7\ \eta_{2/3}^{1/6}\xi_{{\rm e},1/3}^{1/6}\gamma_{{\rm w},4.5}^{-1/6}\beta_{{\rm b},-1}^{-1}$ yr. For $t_{\rm sd} \sim t_{\rm ISM}$ the afterglow emission is close to that of the 'standard' model, where the external medium is the ISM or a stellar wind, which has been extensively and successfully fitted to afterglow observations.

In order to explain the X-ray lines, we need $t_{\rm sd} \lesssim t_{\rm Fe} \sim 1$ yr. This implies that the radio will typically be below the self-absorption frequency, and hence the radio emission from the afterglow would not be detectable. On top of this, the jet break time is given by substituting $n_{\rm H,equiv}$ in place of the external density for a 'standard' external medium (Sari, Piran & Halpern 1999),

$$\begin{aligned}
t_j &= 1.1\left(\frac{1+z}{2}\right)\left(\frac{E_{\rm iso,53}}{n_{\rm H,equiv,0}}\right)^{1/3}\theta_{j,-1}^{8/3}\ {\rm d}\\
&= 0.70\left(\frac{1+z}{2}\right)\left(\frac{E_{\rm iso,53}}{\eta_{2/3}E_{\rm rot,53}}\right)^{1/3}\beta_{{\rm b},-1}t_{{\rm sd},0}\theta_{j,-1}^{8/3}\ {\rm h},
\end{aligned} \tag{96}$$

and is very low for $\theta_{j,-1} = \theta_j/0.1 \sim 1$. If we want to explain the observed values of $t_j \sim 1$ d that are typically observed as resulting from a larger θ_j ($\sim$0.4) then this would imply that the time of transition to a non-relativistic flow should be $t_{\rm NR} \sim \theta_j^{-2}t_j \sim 7t_j \sim 7$d, and in general,

$$t_{\rm NR} \sim \frac{1}{c}\left(\frac{E}{n_{\rm H,equiv}m_{\rm p}c^2}\right)^{1/3} \approx 18\left(\frac{1+z}{2}\right)\left(\frac{E_{51}}{\eta_{2/3}E_{\rm rot,53}}\right)^{1/3}\beta_{{\rm b},-1}t_{{\rm sd},0}\ {\rm d}, \tag{97}$$

where $E = 10^{51}E_{51}$ erg is the true energy of the afterglow, and we have dropped factors of the order of unity. Finally, for $t_{\rm sd} \lesssim t_{\rm Fe} \sim 1$ yr, the transition time from fast to slow cooling is very large, and fast cooling is expected during all of the afterglow.

For $t < t_0$, in the fast cooling regime, the synchrotron flux density, F_ν, is given by[9]

$$F_\nu = F_{\nu,\max}\times\begin{cases}(\nu_{\rm sa}/\nu_{\rm c})^{1/3}(\nu/\nu_{\rm sa})^2 & \nu < \nu_{\rm sa}\\ (\nu/\nu_{\rm c})^{1/3} & \nu_{\rm sa} < \nu < \nu_{\rm c}\\ (\nu/\nu_{\rm c})^{-1/2} & \nu_{\rm c} < \nu < \nu_m\\ (\nu_m/\nu_{\rm c})^{-1/2}(\nu/\nu_m)^{-p/2} & \nu_m < \nu < \nu_M.\end{cases} \tag{98}$$

[9] If there is no significant mixing of the shocked fluid the spectral slope just below $\nu_{\rm sa}$ should be $\nu^{11/8}$, and the familiar ν^2 slope is obtained below a lower break frequency, ν_{ac} (4).

For $t > t_0$ we are in the slow cooling regime, in this case the spectrum peaks at ν_m and again consists of four power-law segments:

$$F_\nu = F_{\nu,\max} \times \begin{cases} (\nu_{\rm sa}/\nu_m)^{1/3}(\nu/\nu_{\rm sa})^2 & \nu < \nu_{\rm sa} \\ (\nu/\nu_m)^{1/3} & \nu_{\rm sa} < \nu < \nu_m \\ (\nu/\nu_m)^{(1-p)/2} & \nu_m < \nu < \nu_{\rm c} \\ (\nu_{\rm c}/\nu_m)^{(1-p)/2}(\nu/\nu_{\rm c})^{-p/2} & \nu_{\rm c} < \nu < \nu_M. \end{cases} \tag{99}$$

6.2 The SSC emission

The SSC emission is calculated similarly to Sections 4.2 and 4.3. The fast cooling spectrum is given by

$$\frac{\nu F_\nu^{\rm SC}}{\nu_m F_{\nu_m}} = Y \times \begin{cases} \left(\nu_{\rm c}^{\rm SC}/\nu_m^{\rm SC}\right)^{1/2}\left(\nu_{\rm sa}^{\rm SC}/\nu_{\rm c}^{\rm SC}\right)^{4/3}\left(\nu/\nu_{\rm sa}^{\rm SC}\right)^2 & \nu < \nu_{\rm sa}^{\rm SC} \\ \left(\nu_{\rm c}^{\rm SC}/\nu_m^{\rm SC}\right)^{1/2}\left(\nu/\nu_{\rm c}^{\rm SC}\right)^{4/3} & \nu_{\rm sa}^{\rm SC} < \nu < \nu_{\rm c}^{\rm SC} \\ \left(\nu/\nu_m^{\rm SC}\right)^{1/2} & \nu_{\rm c}^{\rm SC} < \nu < \nu_m^{\rm SC} \\ \left(\nu/\nu_m^{\rm SC}\right)^{1-p/2} & \nu_m^{\rm SC} < \nu < \nu_{\rm KN,1}^{\rm SC} \\ \left(\nu_{\rm KN,1}^{\rm SC}/\nu_m^{\rm SC}\right)^{1-p/2}(\nu/\nu_{\rm KN,1}^{\rm SC})^{1/2-p} & \nu_{\rm KN,1}^{\rm SC} < \nu < \nu_{\rm KN}^{\rm SC}(\gamma_M), \end{cases} \tag{100}$$

where

$$\nu_m F_{\nu_m} = 3.1 \times 10^{-12}(1+z)\bar{X}^{-1}\epsilon_{{\rm e},-1}^{1/2}\epsilon_{B,-3}^{1/2}E_{\rm iso,53}t_{\rm d}^{-1}d_{L28}^{-2}\ {\rm erg\ cm^{-2}\ s^{-1}}, \tag{101}$$

and for $k = 0$ we have

$$\nu_{\rm sa}^{\rm SC} \approx \gamma_{\rm c}^2\nu_{\rm sa1} \approx 3.9 \times 10^{15}(1+z)^{-3/4}\bar{X}^{-1}\eta_{2/3}^{-3/4}\xi_{{\rm e},1/3}^{3/5}\epsilon_{{\rm e},-1}^{-1/2}\epsilon_{B,-3}^{-3/10}E_{\rm rot,53}^{-3/20}\gamma_{\rm w,4.5}^{-3/5}\beta_{\rm b,-1}^{9/20}t_{\rm sd,1.5}^{9/20}E_{\rm iso,53}^{-1/20}t_{\rm d}^{-1/4}\ {\rm Hz},$$

$$\nu_{\rm c}^{\rm SC} \approx \gamma_{\rm c}^2\nu_{\rm c} \approx 1.5 \times 10^{22}(1+z)^{-3/4}a^{-2}\bar{X}^{-4}\eta_{2/3}^{-9/4}\epsilon_{{\rm e},-1}^{-2}\epsilon_{B,-3}^{-3/2}E_{\rm rot,53}^{-9/4}\beta_{\rm b,-1}^{27/4}t_{\rm sd,1.5}^{27/4}E_{\rm iso,53}^{-5/4}t_{\rm d}^{-1/4}\ {\rm Hz},$$

$$\nu_m^{\rm SC} \approx \gamma_m^2\nu_m \approx 5.1 \times 10^{23}(1+z)^{5/4}\eta_{2/3}^{15/4}\xi_{{\rm e},1/3}^{-4}\epsilon_{{\rm e},-1}^{4}\epsilon_{B,-3}^{1/2}E_{\rm rot,53}^{-1/4}\gamma_{\rm w,4.5}^{4}\beta_{\rm b,-1}^{3/4}t_{\rm sd,1.5}^{3/4}E_{\rm iso,53}^{3/4}t_{\rm d}^{-9/4}\ {\rm Hz}$$

$$\nu_{\rm KN,1}^{\rm SC} \approx \frac{\Gamma_{\rm AG}^2\nu_{\rm KN,0}^2}{\nu_m} \approx 6.7 \times 10^{26}(1+z)^{-7/4}\eta_{2/3}^{-9/4}\xi_{{\rm e},1/3}^{2}\epsilon_{{\rm e},-1}^{-2}\epsilon_{B,-3}^{-1/2}E_{\rm rot,53}^{-1/4}\gamma_{\rm w,4.5}^{-2}\beta_{\rm b,-1}^{3/4}t_{\rm sd,1.5}^{3/4}E_{\rm iso,53}^{-1/4}t_{\rm d}^{3/4}\ {\rm Hz},$$

$$\nu_{\rm KN}^{\rm SC}(\gamma_M) \approx \nu_{\rm KN,0}\Gamma_{\rm AG}\gamma_M \approx 3.8 \times 10^{28}(1+z)^{-13/16}a^{-1/4}\bar{X}^{-1/2}\eta_{2/3}^{-5/16}\epsilon_{{\rm e},-1}^{-1/4}E_{\rm rot,53}^{-5/16}\beta_{\rm b,-1}^{15/16}t_{\rm sd,1.5}^{15/16}E_{\rm iso,53}^{1/16}t_{\rm d}^{-3/16}\ {\rm Hz}, \tag{102}$$

while for $k = 1$ we have

$$\nu_{\rm sa}^{\rm SC} \approx 3.3 \times 10^{15}(1+z)^{-4/5}\bar{X}^{-1}\eta_{2/3}^{-4/5}\xi_{{\rm e},1/3}^{3/5}\epsilon_{{\rm e},-1}^{-1/2}\epsilon_{B,-3}^{-3/10}E_{\rm rot,53}^{-1/5}\gamma_{\rm w,4.5}^{-3/5}\beta_{\rm b,-1}^{2/5}t_{\rm sd,1.5}^{2/5}t_{\rm d}^{-1/5}\ {\rm Hz},$$

$$\nu_{\rm c}^{\rm SC} \approx 1.3 \times 10^{21}(1+z)^{-3/2}a^{-2}\bar{X}^{-4}\eta_{2/3}^{-3}\epsilon_{{\rm e},-1}^{-2}\epsilon_{B,-3}^{-3/2}E_{\rm rot,53}^{-3}\beta_{\rm b,-1}^{6}t_{\rm sd,1.5}^{6}E_{\rm iso,53}^{-1/2}t_{\rm d}^{1/2}\ {\rm Hz},$$

$$\nu_m^{\rm SC} \approx 2.7 \times 10^{23}(1+z)^{7/6}\eta_{2/3}^{11/3}\xi_{{\rm e},1/3}^{-4}\epsilon_{{\rm e},-1}^{4}\epsilon_{B,-3}^{1/2}E_{\rm rot,53}^{-1/3}\gamma_{\rm w,4.5}^{4}\beta_{\rm b,-1}^{2/3}t_{\rm sd,1.5}^{2/3}E_{\rm iso,53}^{5/6}t_{\rm d}^{-13/6}\ {\rm Hz}$$

$$\nu_{\rm KN,1}^{\rm SC} \approx 5.3 \times 10^{26}(1+z)^{-11/6}\eta_{2/3}^{-7/3}\xi_{{\rm e},1/3}^{2}\epsilon_{{\rm e},-1}^{-2}\epsilon_{B,-3}^{-1/2}E_{\rm rot,53}^{-1/3}\gamma_{\rm w,4.5}^{-2}\beta_{\rm b,-1}^{2/3}t_{\rm sd,1.5}^{2/3}E_{\rm iso,53}^{-1/6}t_{\rm d}^{5/6}\ {\rm Hz},$$

$$\nu_{\rm KN}^{\rm SC}(\gamma_M) \approx 2.5 \times 10^{28}(1+z)^{-11/12}a^{-1/4}\bar{X}^{-1/2}\eta_{2/3}^{-5/12}\epsilon_{{\rm e},-1}^{-1/4}E_{\rm rot,53}^{-5/12}\beta_{\rm b,-1}^{5/6}t_{\rm sd,1.5}^{5/6}E_{\rm iso,53}^{1/6}t_{\rm d}^{-1/12}\ {\rm Hz}. \tag{103}$$

The slow cooling spectrum is

$$\frac{\nu F_\nu^{\rm SC}}{\nu_{\rm c} F_{\nu_{\rm c}}} = Y \times \begin{cases} \left(\nu_m^{\rm SC}/\nu_{\rm c}^{\rm SC}\right)^{(3-p)/2}\left(\nu_{\rm sa}^{\rm SC}/\nu_m^{\rm SC}\right)^{4/3}\left(\nu/\nu_{\rm sa}^{\rm SC}\right)^2 & \nu < \nu_{\rm sa}^{\rm SC} \\ \left(\nu_m^{\rm SC}/\nu_{\rm c}^{\rm SC}\right)^{(3-p)/2}\left(\nu/\nu_m^{\rm SC}\right)^{4/3} & \nu_{\rm sa}^{\rm SC} < \nu < \nu_m^{\rm SC} \\ \left(\nu/\nu_{\rm c}^{\rm SC}\right)^{(3-p)/2} & \nu_m^{\rm SC} < \nu < \nu_{\rm c}^{\rm SC} \\ \left(\nu/\nu_{\rm c}^{\rm SC}\right)^{1-p/2} & \nu_{\rm c}^{\rm SC} < \nu < \nu_{\rm KN,1}^{\rm SC} \\ \left(\nu_{\rm KN,1}^{\rm SC}/\nu_{\rm c}^{\rm SC}\right)^{1-p/2}\left(\nu/\nu_{\rm KN,1}^{\rm SC}\right)^{-(p+1)/2} & \nu_{\rm KN,1}^{\rm SC} < \nu < \nu_{\rm KN}^{\rm SC}(\gamma_M), \end{cases} \tag{104}$$

where $\nu_{\rm c}F_{\nu_{\rm c}}$ is just $a = (\nu_m/\nu_{\rm c})^{(2-p)/2}$ times $\nu_m F_{\nu_m}$ for the fast cooling, which is given in equation (101). For $k = 0$ we have

$$\nu_{\rm sa}^{\rm SC} \approx \gamma_m^2\nu_{\rm sa2} \approx 1.1 \times 10^{16}(1+z)^{-1/4}\eta_{2/3}^{3/4}\xi_{{\rm e},1/3}^{-2/5}\epsilon_{{\rm e},-1}\epsilon_{B,-3}^{1/5}E_{\rm rot,53}^{7/20}\gamma_{\rm w,4.5}^{2/5}\beta_{\rm b,-1}^{-21/20}t_{\rm sd,1.5}^{-21/20}E_{\rm iso,53}^{9/20}t_{\rm d}^{-3/4}\ {\rm Hz},$$

$$\nu_{\rm KN,1}^{\rm SC} = \frac{\Gamma_{\rm AG}^2\nu_{\rm KN,0}^2}{\nu_{\rm c}} \approx 3.8 \times 10^{27}(1+z)^{-3/4}a\bar{X}^2\eta_{2/3}^{3/4}\epsilon_{{\rm e},-1}\epsilon_{B,-3}^{1/2}E_{\rm rot,53}^{3/4}\beta_{\rm b,-1}^{-9/4}t_{\rm sd,1.5}^{-9/4}E_{\rm iso,53}^{3/4}t_{\rm d}^{-1/4}\ {\rm Hz}, \tag{105}$$

and for $k = 1$ we obtain

$$\nu_{\rm sa}^{\rm SC} \approx 1.4\times 10^{16}(1+z)^{-2/15}\eta_{2/3}^{13/15}\xi_{{\rm e},1/3}^{-2/5}\epsilon_{{\rm e},-1}\epsilon_{B,-3}^{1/5}E_{\rm rot,53}^{7/15}\gamma_{\rm w,4.5}^{2/5}\beta_{\rm b,-1}^{-14/15}t_{\rm sd,1.5}^{-14/15}E_{\rm iso,53}^{1/3}t_{\rm d}^{-13/15}\ {\rm Hz},$$
$$\nu_{\rm KN,1}^{\rm SC} \approx 7.6\times 10^{27}(1+z)^{-1/2}a\bar{X}^2\eta_{2/3}\epsilon_{{\rm e},-1}\epsilon_{B,-3}^{1/2}E_{\rm rot,53}\beta_{\rm b,-1}^{-2}t_{\rm sd,1.5}^{-2}E_{\rm iso,53}^{1/2}t_{\rm d}^{-1/2}\ {\rm Hz}. \tag{106}$$

6.3 The EC emission

The EC emission in this case arises from the upscattering of the plerion radiation by the relativistic electrons behind the afterglow shock. We provide detailed expressions for one representative plerion spectrum, the one given in equation (24). This spectrum is the spectrum for 12 yr $\sim t_2 < t_{\rm sd} < t_3 \sim 65$ yr (see equations 35 and 23), which is of most interest. Similar expressions for the other plerion spectra can be readily derived in a similar manner. We note that for $t_{\rm sd} < t_2$ the synchrotron emission of the plerion near the peak of νF_ν is the same as for the spectrum we use (i.e. for $t_2 < t_{\rm sd} < t_3$), and therefore the EC near the peak of its νF_ν should be the same. The peak of νF_ν for the SSC plerion emission is typically above the KN limit for the AG electrons, and should therefore have a negligible contribution for the EC emission of the afterglow. The resulting EC spectrum depends on whether the electrons in the afterglow shock are in the fast cooling or slow cooling regime. The EC spectrum is

$$\frac{\nu F_\nu^{EC}}{a\nu_m F_{\nu_m}} = X\times\begin{cases}\left(\nu_{\rm c}^{EC}/\nu_m^{EC}\right)^{1/2}\left(\nu_{\rm sa}^{EC}/\nu_{\rm c}^{EC}\right)^{4/3}\left(\nu/\nu_{\rm sa}^{EC}\right)^2 & \nu<\nu_{\rm sa}^{EC}\\ \left(\nu_{\rm c}^{EC}/\nu_m^{EC}\right)^{1/2}\left(\nu/\nu_{\rm c}^{EC}\right)^{4/3} & \nu_{\rm sa}^{EC}<\nu<\nu_{\rm c}^{EC}\\ \left(\nu/\nu_m^{EC}\right)^{1/2} & \nu_{\rm c}^{EC}<\nu<\nu_m^{EC}\\ \left(\nu/\nu_m^{EC}\right)^{1-s/2} & \nu_m^{EC}<\nu<\nu_{\rm KN}^{EC}(\gamma_M),\end{cases} \tag{107}$$

where $\nu_{\rm KN}^{EC}(\gamma_M) = \nu_{\rm KN}^{\rm SC}(\gamma_M)$ is given by equation (102). For fast cooling and $k = 0$

$$\nu_{\rm sa}^{EC} \approx \Gamma_{\rm AG}^2\gamma_{\rm c}^2\nu_{\rm bsa} \approx 2.4\times 10^{18}(1+z)^{-1/2}\frac{\xi_{{\rm e},1/3}^{1/3}\epsilon_{{\rm b}B,-3}^{1/6}\beta_{\rm b,-1}^{23/6}t_{\rm sd,1.5}^{7/2}}{\bar{X}^2\eta_{2/3}^{3/2}\epsilon_{{\rm be},1/3}^{1/6}\epsilon_{{\rm e},-1}\epsilon_{B,-3}E_{\rm rot,53}^{7/6}\gamma_{\rm w,4.5}^{1/3}E_{\rm iso,53}^{1/2}t_{\rm d}^{1/2}}\ {\rm Hz},$$
$$\nu_{\rm c}^{EC} \approx \Gamma_{\rm AG}^2\gamma_{\rm c}^2\nu_{\rm bc} \approx 6.4\times 10^{19}(1+z)^{-1/2}\frac{\beta_{\rm b,-1}^{9}t_{\rm sd,1.5}^{7}}{\bar{X}^2\eta_{2/3}^{3}\epsilon_{{\rm be},1/3}^{1/2}\epsilon_{{\rm b}B,-3}\epsilon_{{\rm e},-1}\epsilon_{B,-3}E_{\rm rot,53}^{3}E_{\rm iso,53}^{1/2}t_{\rm d}^{1/2}}\ {\rm Hz}, \tag{108}$$
$$\nu_m^{EC} \approx \Gamma_{\rm AG}^2\gamma_m^2\nu_{{\rm b}m} \approx 6.5\times 10^{21}(1+z)^{1/2}\eta_{2/3}^4\xi_{{\rm e},1/3}^{-4}\epsilon_{{\rm be},1/3}^2\epsilon_{{\rm b}B,-3}^{1/2}\epsilon_{{\rm e},-1}^2\gamma_{\rm w,4.5}^4E_{\rm iso,53}^{1/2}t_{\rm d}^{-3/2}\ {\rm Hz},$$

while for fast cooling with $k = 1$ we have

$$\nu_{\rm sa}^{EC} \approx 4.1\times 10^{17}(1+z)^{-1}\bar{X}^{-2}\eta_{2/3}^{-2}\xi_{{\rm e},1/3}^{1/3}\epsilon_{{\rm be},1/3}^{-1/6}\epsilon_{{\rm b}B,-3}^{1/6}\epsilon_{{\rm e},-1}^{-1}\epsilon_{B,-3}^{-1}E_{\rm rot,53}^{-5/3}\gamma_{\rm w,4.5}^{-1/3}\beta_{\rm b,-1}^{10/3}t_{\rm sd,1.5}^{3}\ {\rm Hz},$$
$$\nu_{\rm c}^{EC} \approx 1.1\times 10^{19}(1+z)^{-1}\bar{X}^{-2}\eta_{2/3}^{-7/2}\epsilon_{{\rm be},1/3}^{-1}\epsilon_{{\rm b}B,-3}^{-1/2}\epsilon_{{\rm e},-1}^{-1}\epsilon_{B,-3}^{-1}E_{\rm rot,53}^{-7/2}\beta_{\rm b,-1}^{17/2}t_{\rm sd,1.5}^{13/2}\ {\rm Hz},$$
$$\nu_m^{EC} \approx 2.7\times 10^{21}(1+z)^{1/3}\eta_{2/3}^{23/6}\xi_{{\rm e},1/3}^{-4}\epsilon_{{\rm be},1/3}^2\epsilon_{{\rm b}B,-3}^{1/2}\epsilon_{{\rm e},-1}^2E_{\rm rot,53}^{-1/6}\gamma_{\rm w,4.5}^4\beta_{\rm b,-1}^{-5/6}t_{\rm sd,1.5}^{-5/6}E_{\rm iso,53}^{2/3}t_{\rm d}^{-4/3}\ {\rm Hz}. \tag{109}$$

For slow cooling with $k = 0$ we have

$$\nu_{\rm sa}^{EC} \approx \Gamma_{\rm AG}^2\gamma_m^2\nu_{\rm bsa} \approx 1.4\times 10^{19}(1+z)^{1/2}\frac{\eta_{2/3}^{3/2}\epsilon_{{\rm b}B,-3}^{1/6}\epsilon_{{\rm e},-1}^2\gamma_{\rm w,4.5}^{5/3}\beta_{\rm b,-1}^{5/6}t_{\rm sd,1.5}^{1/2}E_{\rm iso,53}^{1/2}}{\xi_{{\rm e},1/3}^{5/3}\epsilon_{{\rm be},1/3}^{1/6}E_{\rm rot,53}^{1/6}t_{\rm d}^{3/2}}\ {\rm Hz},$$
$$\nu_{\rm c}^{EC} \approx \Gamma_{\rm AG}^2\gamma_m^2\nu_{\rm bc} \approx 3.7\times 10^{20}(1+z)^{1/2}\frac{\epsilon_{{\rm e},-1}^2\gamma_{\rm w,4.5}^2\beta_{\rm b,-1}^6t_{\rm sd,1.5}^4E_{\rm iso,53}^{1/2}}{\xi_{{\rm e},1/3}^2\epsilon_{{\rm be},1/3}\epsilon_{{\rm b}B,-3}^{1/2}E_{\rm rot,53}^2t_{\rm d}^{3/2}}\ {\rm Hz},$$
$$\nu_m^{EC} \approx \Gamma_{\rm AG}^2\gamma_{\rm c}^2\nu_{{\rm b}m} \approx 1.1\times 10^{21}(1+z)^{-1/2}\frac{\eta_{2/3}\epsilon_{{\rm be},1/3}^2\epsilon_{{\rm b}B,-3}^{1/2}\gamma_{\rm w,4.5}^2\beta_{\rm b,-1}^3t_{\rm sd,1.5}^3}{a\bar{X}^2\xi_{{\rm e},1/3}^2\epsilon_{{\rm e},-1}\epsilon_{B,-3}E_{\rm rot,53}E_{\rm iso,53}^{1/2}t_{\rm d}^{1/2}}\ {\rm Hz}, \tag{110}$$

and finally for $k = 1$ we have

$$\nu_{\rm sa}^{EC} \approx 5.8\times 10^{18}(1+z)^{1/3}\eta_{2/3}^{4/3}\xi_{{\rm e},1/3}^{-5/3}\epsilon_{{\rm be},1/3}^{-1/6}\epsilon_{{\rm b}B,-3}^{1/6}\epsilon_{{\rm e},-1}^2E_{\rm rot,53}^{-1/3}\gamma_{\rm w,4.5}^{5/3}\beta_{\rm b,-1}^{2/3}t_{\rm sd,1.5}^{1/3}E_{\rm iso,53}^{2/3}t_{\rm d}^{-4/3}\ {\rm Hz},$$
$$\nu_{\rm c}^{EC} \approx 1.6\times 10^{20}(1+z)^{1/3}\eta_{2/3}^{-1/6}\xi_{{\rm e},1/3}^{-2}\epsilon_{{\rm be},1/3}^{-1}\epsilon_{{\rm b}B,-3}^{-1/2}\epsilon_{{\rm e},-1}^2E_{\rm rot,53}^{-13/6}\gamma_{\rm w,4.5}^2\beta_{\rm b,-1}^{35/6}t_{\rm sd,1.5}^{23/6}E_{\rm iso,53}^{2/3}t_{\rm d}^{-4/3}\ {\rm Hz},$$
$$\nu_m^{EC} \approx 1.9\times 10^{20}(1+z)^{-1}a^{-1}\bar{X}^{-2}\eta_{2/3}^{1/2}\xi_{{\rm e},1/3}^{-2}\epsilon_{{\rm be},1/3}^2\epsilon_{{\rm b}B,-3}^{1/2}\epsilon_{{\rm e},-1}^{-1}\epsilon_{B,-3}^{-1}E_{\rm rot,53}^{-3/2}\gamma_{\rm w,4.5}^2\beta_{\rm b,-1}^{5/2}t_{\rm sd,1.5}^{5/2}\ {\rm Hz}. \tag{111}$$

6.4 High-energy emission

Fig. 2 shows the νF_ν spectrum of the afterglow at $t = 500$ s and 5×10^3 s, for our fiducial parameters, and for $t_{\rm sd} = 20$ yr, $E_{\rm rot,53} = 0.5$, $z = 1$, $R_{\rm s}/R_{\rm b} = 0.1$. As can be seen from the figure, for $t = 500$ s (5×10^3 s) the synchrotron is dominant below 45 MeV (2 MeV), while the EC

is dominant above this range. At $t = 5 \times 10^3$ s the SSC component becomes dominant above 40 GeV. We expect an upper cut-off at $h\nu_{\gamma\gamma} \sim$ 250 GeV, owing to opacity to pair production, with the photons of the plerion. This upper cut-off moves down to a lower energy for smaller values of $t_{\rm sd}$, and is ~1 GeV for $t_{\rm sd} = 1$ yr $\sim t_{\rm Fe}$. This implies that for afterglows with X-ray line features we expect no high-energy emission above this limit.

We find that the early afterglow ($t \lesssim 100$ s) emission at $\gtrsim 100$ MeV is dominated by the EC and SSC component, which are comparable at this time. At later times the EC becomes dominant over the SSC component. The peak of the νF_ν^{EC} emission is at the level of $\sim 5 \times 10^{-9} (t/500\ {\rm s})^{-1}$ erg cm^{-2}s^{-1}, and is located at $h\nu_m^{EC} \sim 70\ (t/500\ {\rm s})^{-3/2}$ GeV (see equation 108). The spectrum scales as $\nu F_\nu \propto \nu^{(2-s)/2}$ above this photon energy, implying a flat νF_ν for values of $s \sim 2$ that are typically inferred for PWBs, while it scales as $\nu F_\nu \propto \nu^{1/2}$ below this energy. At early times the afterglow radius is relatively small ($R_{\rm AG} \lesssim f R_{\rm b}$), so that X is approximately constant in time, and the peak of the νF_ν EC spectrum has a temporal scaling similar to that for the synchrotron component (i.e. $\propto t^{-1}$, see equation 101). We therefore expect νF_ν at a fixed photon energy to decay very slowly with time, as $t^{-1/4}$, at $\nu < \nu_m^{EC}$, and decay approximately linearly with time ($\propto t^{-1-3(s-2)/4}$) at $\nu > \nu_m^{EC}$. The temporal decay becomes larger than these scalings as the afterglow radius $R_{\rm AG}$ increases above $f R_{\rm b}$, and the parameter X begins to decrease with time.

This result can explain the high-energy emission detected by EGRET for GRB 940217 (Hurley et al. 1994). This detection consists of photons of energies $\gtrsim 50$ MeV, where 10 photons were observed during the prompt GRB emission, that lasted 180s, and 18 photons were detected up to 5400 s after the end of the GRB, which include a photon of energy 18 GeV. During the post-GRB emission, the source position was Earth-occulted for ~3700 s. At $t \sim 500$ s the flux is ~1–2 $\times 10^{-9}$ erg cm^{-2}s^{-1} which is roughly consistent with our results. At $t \sim 5000$ s, after the Earth occultation, the flux is a factor of ~2–3 lower, if we exclude the one 18 GeV photon. This moderate time decay is consistent with our results.

A different interpretation for the high-energy emission discussed above was recently suggested by Wang et al. (2002), in the similar context of the supranova model, where the GRB occurs inside a plerionic environment. The main difference is that they consider a pulsar wind that consists purely of e$^\pm$ pairs, which is in the fast cooling regime, and therefore the radius of the termination shock of the wind, $R_{\rm s}$ is very close to the outer radius of the PWB, $R_{\rm b}$, and all the shocked wind is concentrated within a thin radial interval, $R_{\rm b} - R_{\rm s} \ll R_{\rm b}$. They try to explain the high-energy emission as the synchrotron emission from the early afterglow. They obtain $h\nu_m \sim 1$ GeV at $t \sim 180$ s, and according to their model $t \sim R_{\rm b}/2\Gamma^2 c$ or $\Gamma \propto t^{-1/2}$ and $\nu_m \propto \Gamma^4 \propto t^{-2}$. However, this implies $h\nu_m \sim$ a few keV after 1 day, which is inconsistent with afterglow observations. They also claim that the EC emission is unimportant, which is in contradiction with our conclusions. The inclusion of a proton component in the pulsar wind with a similar energy to that of the e$^\pm$ component allows only the energy in the e$^\pm$ to be radiated away, so that even for a fast cooling PWB a large part of the energy of the pulsar wind remains in the protons and $R_{\rm s}$ is significantly smaller than $R_{\rm b}$.

7 DISCUSSION

We have studied the observational implications of GRBs occurring inside a pulsar wind bubble, as is expected in the supranova model. We find that the most important parameter that determines the behaviour of the system is the time delay, $t_{\rm sd}$, between the supernova and GRB events. The value of $t_{\rm sd}$ is given by the typical time-scale on which the SMNS loses its rotational energy as a result of magnetic dipole radiation (see equation 2) and depends mainly on the magnetic field strength of the SMNS, B_* (since its mass, radius and spin period are constrained to a much smaller range of possible values). For $B_* \sim 10^{12}$–10^{13} G, $t_{\rm sd}$ is between a few weeks and several years. However, a larger range in B_*, and correspondingly in $t_{\rm sd}$, seems plausible. We therefore consider $t_{\rm sd}$ as a free parameter, and predict the observational consequences of different values for this parameter.

(i) For extremely small values of $t_{\rm sd} < t_{\rm col} = R_\star/\beta_{\rm b} c \approx 0.9 R_{\star,13} \beta_{\rm b,-1}^{-1}$ h, where $R_\star = 10^{13} R_{\star,13}$ cm is the radius of the progenitor star (before it explodes in a supernova), the stellar envelope does not have enough time to increase its radius considerably before the GRB goes off, and the supranova model reduces to the collapsar model. In this respect, the collapsar model may be seen to be a special case of the supranova model. Such low values of $t_{\rm sd}$ might be achieved if the SMNS is not rotating uniformly, as differential rotation may amplify the magnetic field to very large values.

(ii) When $t_{\rm col} < t_{\rm sd} < t_{\rm IS} \sim 3\beta_{\rm b}^{-1} t_v \Gamma^{2(4-k)/(3-k)} \approx 16 \beta_{\rm b,-1}^{-1} \Gamma_{2.5}^{8/3} t_{v,-2}$ d (for $k = 0$) the deceleration radius $R_{\rm dec} \sim R_{\rm NR} \Gamma^{-2/(3-k)} \sim R_{\rm b}\ \Gamma^{-2/(3-k)}$ is smaller than the radius for internal shocks $R_{\rm IS} \sim 2\Gamma^2 c t_v$. In this case the kinetic energy of the GRB ejecta is dissipated through an external shock that is driven into the shocked pulsar wind, before internal shocks that result from variability within the outflow have time to occur. For an elongated PWB, $t_{\rm IS}$ can be smaller by up to a factor of ~10, since the polar radius would be ~10 times larger for the same $t_{\rm sd}$, and the volume of the PWB would be much larger and the density much smaller.

(iii) If $t_{\rm IS} < t_{\rm sd} < t_\tau \sim 0.4$ yr, an internal shock can occur inside the PWB, but the SNR shell is still optically thick to Thomson scattering, and the radiation from the plerion, the prompt GRB and the afterglow cannot escape and reach the observer. If the SNR shell is clumpy (possibly owing to the Rayleigh–Taylor instability, see Section 2), then the Thomson optical depth in the underdense regions within the shell may decrease below unity at $t_{\rm sd}$ somewhat smaller than t_τ, enabling some of the radiation from the plerion to escape. For an elongated PWB, the polar radius can be larger by up to a factor of ~10, which reduces t_τ by the same factor. Furthermore, the elongation can be caused by a smaller than average surface mass density of the SNR shell at the poles. This would further reduce t_τ.

(iv) For $t_\tau < t_{\rm sd} < t_{\rm Fe} \sim 1$ yr the SNR shell has a Thomson optical depth smaller than unity, but the optical depth for the iron line features is still $\gtrsim 1$ so that detectable X-ray line features, such as the iron lines observed in several afterglows, can be produced.

(v) Finally, for $t_{\rm Fe} < t_{\rm sd}$, we expect no iron lines. When $t_{\rm sd}$ is between ~2 and ~20 yr the radio emission of the plerion may be detectable for $\gamma_{\rm w} \lesssim 10^5$. The lack of detection of such a radio emission excludes values of $t_{\rm sd}$ in this range, if indeed $\gamma_{\rm w} \lesssim 10^5$, as is needed to obtain reasonable values for the break frequencies of the afterglow. For $t_{\rm sd} = t_{\rm ISM} \sim 38$ yr, the effective density of the PWB is similar to that of the ISM (i.e. 1 cm^{-3}), and the afterglow emission is similar to that of the standard model, where $k = 0$ is similar to an ISM environment, with the exception that in our model a value of $k = 1$, that is intermediate between an ISM and a stellar wind, is also possible. Larger (smaller) values of the external density are obtained for smaller (larger) values of $t_{\rm sd}$.

The SNR shell is decelerated owing to the sweeping up of the surrounding medium for $t_{\rm sd} > 225\ M_{\rm SNR,1}^{1/3} n_0^{-1/3} \beta_{\rm b,-1}^{-1}$ yr, where $n = n_0$ cm^{-3} is the number density of the external medium, which is larger than the values of $t_{\rm sd}$ that are of interest to us. This effect may therefore be neglected for our purposes.

An important difference between our analysis and previous works (KG; IGP) is that we allow for a proton component in the pulsar wind, which carries a significant fraction of its energy. In contrast to the e$^\pm$ component, the internal energy of the protons in the shocked wind is not radiated away, and therefore a large fraction of the energy in the pulsar wind (~10^{53} erg) is always left in the PWB. This implies that even for a fast cooling PWB, the radius of the wind termination shock $R_{\rm s}$ is significantly smaller than the radius of the SNR, $R_{\rm b}$, and that the afterglow shock typically becomes non-relativistic before it reaches the outer boundary of the PWB.

8 CONCLUSIONS

Our main conclusion is that existing afterglow observations set interesting constraints on the model parameters, the most important of which is the time delay $t_{\rm sd}$ between the supernova and GRB events, which is constrained to be $\gtrsim 20$ yr, in order to explain typical afterglow observations and the lack of detection of the plerion emission in the radio during the afterglow. Another important conclusion is that iron line features that have been observed in a few X-ray afterglows cannot be naturally explained within the simplest spherical version of the PWB model that has been considered in this work. This is because the production of these lines requires $t_{\rm sd} \lesssim t_{\rm Fe} \sim 1$ yr, which implies a very large density for the PWB and effects the afterglow emission in a number of different ways: (i) the self-absorption frequency of the afterglow is typically above the radio band, implying no detectable radio afterglow, while radio afterglows were detected for GRBs 970508, 970828 and 991216, where the iron line feature for the latest of these three is the most significant detection to date (~4σ). We also expect the self-absorption frequency of the plerion emission to be above the radio in this case, so that the radio emission from the plerion should not be detectable, and possibly confused with that of the afterglow. (ii) A short jet break time t_j and a relatively short non-relativistic transition time $t_{\rm NR}$ are implied, as both scale linearly with $t_{\rm sd}$ and are in the right range inferred from observations for $t_{\rm sd} \sim 30$ yr (see equations 96 and 97). (iii) The electrons are always in the fast cooling regime during the entire afterglow.

The above constraints regarding the iron lines may be relaxed if we allow for deviations from the simple spherical geometry we have assumed for the PWB. A natural variant is when the PWB becomes elongated along its rotational axis (KG). This may occur if the surface mass density of the SNR shell is smaller at the poles compared with the equator, so that during the acceleration of the SNR shell by the pressure of the shocked pulsar wind (which is expected to be roughly the same at the poles and at the equator) its radius will become larger at the poles, as the acceleration there will be larger. A large-scale toroidal magnetic field within the PWB may also contribute to the elongation of the SNR shell along its polar axis (KG). It is also likely that the progenitor star that gave rise to an SMNS had an anisotropic mass loss, which results in a density contrast between the equators (where the density is higher) and the poles (where the density is lower). A sufficiently large density contrast between the equator and the poles can also contribute to the elongation of the shell, for sufficiently large $t_{\rm sd}$, as the SNR shell will begin to be decelerated owing to the interaction with the external medium, at a smaller radius near the equator, compared with the poles. A similar non-spherical variant of the model is if we allow for holes in the SNR shell, that extend over a small angle around the polar axis, where all the wind is decelerated in a termination shock within the SNR shell ($R_{\rm s} < R_{\rm b}$), but most of the shocked pulsar wind can get out through the holes near the poles and reach a radius considerably larger than $R_{\rm b}$. This variant may be viewed as a limiting case of the previous variant, when the surface density contrast of the SNR shell, between the equator and the poles is very large. This implies that most of the mass in the SNR shell is concentrated near the equator, while only a small fraction of it is near the poles, so the radius near the poles can be as large as $\sim ct_{\rm sd}$, while the equatorial radius is $\lesssim R_{\rm b}$. In both variants, the total volume of the PWB is close to that of a sphere with the polar radius, and much larger than that of a sphere with the equatorial radius. This would allow for a smaller density with the same small value of the equatorial radius that is required to produce the iron lines. We see that in principle, variants of the simple model are capable of reconciling between the iron line detections and the afterglow observations.

An important advantage of the PWB model is that it can naturally explain the large values of ϵ_B and $\epsilon_{\rm e}$ that are inferred from fits to afterglow data (KG), thanks to the large relative number of electron–positron pairs and large magnetic fields in the PWB. This is in contrast with a standard environment that is usually assumed to be either an ISM or the stellar wind of a massive progenitor, that consists of protons and electrons, and where the magnetic field is too small to explain the values inferred from afterglow observations, and magnetic field generation at the shock itself is required. Additional advantages of the PWB model are its ability to naturally account for the range of external densities inferred from afterglow fits, and allowing for a homogeneous external medium ($k \sim 0$), as inferred for most afterglows, with a massive star progenitor.

Another advantage of the PWB model is its capability of explaining the high-energy emission observed in some GRBs (Schneid et al. 1992, 1995; Hurley et al. 1994; Sommer et al. 1994). We find that the high-energy emission during the early afterglow at photon energies $\gtrsim$100 keV is dominated by the external Compton component, which is as a result of the upscattering of photons from the plerion radiation field to higher energies by the relativistic electrons behind the afterglow shock. We predict that such a high-energy emission may be detected in a large fraction of GRBs with the upcoming mission GLAST. However, we find an upper cut-off at a photon energy of $\sim 1\, t_{\rm sd,0}^2$ GeV, owing to opacity to pair production with the photons of the PWB. This implies no high-energy emission above $\sim$1 GeV for afterglows with X-ray line features, but allows photons up to an energy of $\sim$1TeV for afterglows with an external density typical of the ISM ($t_{\rm sd} \sim t_{\rm ISM}$).

ACKNOWLEDGMENTS

We thank Arieh Königl for his careful reading of the manuscript and helpful comments. This research was supported by the partial support of the Italian Ministry for University and Research (MIUR) through the grant Cofin-01-02-43 (DG) and by the grant NSF PHY 00-70928 (JG). We thank the Einstein Centre at the Weizmann Institute of Science for the hospitality and for the pleasant working atmosphere. DG thanks the Institute for Advanced Study, where most of this research was carried out, for the hospitality and the nice working atmosphere.

REFERENCES

Amati L. et al., 2000, Sci, 290, 953
Antonelli L. et al., 2000, ApJ, 545, L39
Arons J., 2002, in Slane P.O., Gaensler B.M., eds, ASP Conf. Ser. Vol. 271, Neutron Stars in Supernova Remnants. Astron. Soc. Pac., San Francisco, p. 71
Borozdin K., Trudolyubov S., 2003, ApJ, 583, L57
Böttcher M., Fryer C.L., Dermer C.D., 2002, ApJ, 567, 441
Chevalier R.A., Li Z.-Y., 2000, ApJ, 536, 195
Cook G.B., Shapiro S.L., Teukolsky S.A., 1994, ApJ, 424, 823
Eichler D., Livio M., Piran T., Schramm D.N., 1989, Nat, 340, 126
Emmering R.T., Chevalier R.A., 1987, ApJ, 321, 334
Frail D. et al., 2001, ApJ, 562, L55
Fryer C., Woosley S.E., 1998, ApJ, 502, L9
Fryer C., Woosley S.E., Hartmann D.H., 1999, ApJ, 526, 152
Gallant Y.A., Arons J., 1994, ApJ, 435, 230
Ghisellini G., Lazzati D., Celotti A., Rees M.J., 2000, MNRAS, 316, L45
Ghisellini G., Lazzati D., Rossi E., Rees M.J., 2002, A&A, 389, L33
Granot J., Königl A., 2001, ApJ, 560, 145
Granot J., Sari R., 2002, ApJ, 568, 820
Granot J., Piran T., Sari R., 1999, ApJ, 527, 236
Granot J., Piran T., Sari R., 2000, ApJ, 534, L163
Haensel P., Lasota J.-P., Zdunik J.L., 1999, A&A, 344, 155
Helfand D.J., Gotthelf E.V., Halpern J.P., 2001, ApJ, 556, 380
Hurley K. et al., 1994, Nat, 372, 652
Inoue S., Guetta D., Pacini F., 2003, ApJ, 583, 379 (IGP)
Jun B.-I., 1998, ApJ, 499, 282
Kennel C.F., Coroniti F.V., 1984, ApJ, 283, 694
Königl A., Granot J., 2002, ApJ, 574, 134 (KG)
Krolik J., Kallman T., 1987, ApJ, 320, L5
Lazzati D., Campana S., Ghisellini G., 1999, MNRAS, 304, L31
Lazzati D., Ghisellini G., Celotti A., Rees M.J., 2000, ApJ, 529, L17
Lazzati D., Ghisellini G., Amati L., Frontera F., Vietri M., Stella L., 2001, ApJ, 556, 471
Narayan R., Paczński B., Piran T., 1992, ApJ, 395, L83
Pacini F., 1967, Nat, 216, 567
Paczński B., 1998, ApJ, 494, 45
Panaitescu A., Kumar P., 2000, ApJ, 543, 66
Panaitescu A., Kumar P., 2002, ApJ, 571, 779
Piro L. et al., 1998, A&A, 331, L41
Piro L. et al., 2000, Sci, 290, 955
Rees M.J., Gunn J.E., 1974, MNRAS, 167, 1
Rees M.J., Mészáros P., 1994, ApJ, 430, L93
Reeves J.N. et al., 2002, Nat, 416, 512
Reynolds S.P., Chevalier R.A., 1984, ApJ, 278, 630
Rutledge R., Sako M., 2003, MNRAS, in press (astro-ph/0206073)
Salgado M., Bonazzola S., Gourgoulmon E., Haensel P., 1994, A&A, 291, 155
Sari R., Esin A.A., 2001, ApJ, 548, 787
Sari R., Piran T., 1997, ApJ, 485, 270
Sari R., Narayan R., Piran T., 1996, ApJ, 473, 204
Sari R., Piran T., Narayan R., 1998, ApJ, 497, L17
Sari R., Piran T., Halpern J., 1999, ApJ, 519, L17

Schneid E.J. et al., 1992, A&A, 255, L13
Schneid E.J. et al., 1995, ApJ, 453, 95
Sommer M. et al., 1994, ApJ, 422, L63
Vietri M., Stella L., 1998, ApJ, 507, L45
Vietri M. et al., 2001, ApJ, 550, L43
Vreeswijk P.M. et al., 1999, GCN Circ. 496, http://gcn.gsfc.nasa.gov/gcn/gcn3/496.gcn3
Wang X.Y., Dai Z.G., Lu T., 2002, MNRAS, 336, 803
Wijers R.A.M.J., Galama T.J., 1999, ApJ, 523, 177
Woosley S.E., 1993, ApJ, 405, 273
Yoshida A. et al., 2001, ApJ, 557, L27

This paper has been typeset from a TEX/LATEX file prepared by the author.